

**GPR183 Expression on Pulmonary Conventional Dendritic
Cell Type 2 Dictates Subtissular Localisation and Instructs
Their Survival via the Thymic Stromal Lymphopoietin (TSLP)
– TSLP Receptor (TSLPR) Axis**

Dissertation
zur
Erlangung des Doktorgrades (Dr. rer. nat.)
der
Mathematisch-Naturwissenschaftlichen Fakultät
der
Rheinischen Friedrich-Wilhelms-Universität Bonn

vorgelegt von

Lili Zhang

aus

Shandong (China)

Bonn (12, 2020)

Angefertigt mit Genehmigung der Mathematisch-Naturwissenschaftlichen Fakultät
der Rheinischen Friedrich-Wilhelms-Universität Bonn

Erstgutachter: Prof. Dr. Andreas Schlitzer

Zweitgutachterin: Prof. Dr. Christa E. Müller

Tag der Promotion: 26.03.2021

Erscheinungsjahr: 2021

I Believe That

Science is Real & DC is Cool!

Index

Index.....	I
Abstract	V
List of abbreviations	VII
1 Introduction	1
1.1 Dendritic cells (DCs) link innate and adaptive immunity	1
1.2 Phenotypic diversity and functional division within DCs networks	1
1.2.1 Phenotype and function of pDCs	2
1.2.2 Phenotype and function of cDCs	2
1.2.2.1 Phenotype and function of cDC1s.....	3
1.2.2.2 Phenotypic diversity and functional division of cDC2s.....	3
1.2.3 Phenotype and function of inf-DCs	5
1.3 Ontogeny of DCs: from BM progenitors to DC subsets in tissues.....	5
1.4 The mononuclear phagocyte system (MPS) strategically locates within different sites of the lung	7
1.5 GPR183 and its ligand $7\alpha,25\text{-OHC}$	8
1.6 Immune regulation of GPR183 – oxysterol ($7\alpha,25\text{-OHC}$) axis.....	10
2 Materials and methods	13
2.1 Materials.....	13
2.1.1 Mice.....	13
2.1.2 Consumables	13
2.1.3 Equipment	14

2.1.4 Reagents and kits	15
2.1.5 Buffers	17
2.1.6 Antibodies used for FACS and histology staining	18
2.2 Methods	20
2.2.1 Isolation of cells from blood, BM and lung	20
2.2.2 PFA-fixed, paraffin embedded lung for histology staining	20
2.2.3 Hematoxylin and eosin (HE) staining	20
2.2.4 Alcian blue and nuclear fast red staining.....	21
2.2.5 Quantitative real time (RT)-PCR.....	21
2.2.6 Immunofluorescence microscopy	22
Lung preparation.....	22
Lung section	22
Staining.....	22
2.2.7 Flow cytometry.....	23
Surface staining	23
Intra-cellular staining.....	23
Intra-nuclear staining.....	23
Apoptosis staining.....	24
2.2.8 Culture of BM derived DC.....	24
2.2.9 Generation of BM chimeras.....	24
2.2.10 NicheNet analysis: potential interactions between ligands from adventitial fibroblasts and target genes from <i>Mgl2</i> ⁺ cDC2 cells.....	24
2.2.11 Statistics	25

3	Results	26
3.1	Flow cytometric characterization of pulmonary mononuclear phagocytes.....	26
3.2	<i>Gpr183</i> is abundantly expressed in cDCs, not in stromal cells	29
3.3	<i>Gpr183</i> ⁺ cDC2s show higher expression of maturation and proliferation in the murine lung	32
3.4	Genetic deletion of <i>Gpr183</i> leads to a deficiency in pulmonary cDC2 during homeostasis.....	32
3.5	GPR183 deletion results in a diminished migratory cDC2 compartment in the mediastinal lymph node.....	35
3.6	Intrinsic expression of GPR183 is crucial for pulmonary cDC2 maintenance	36
3.7	DC specific ablation of GPR183 decreases pulmonary cDC2 proliferation ...	39
3.8	GPR183 expression is not required for normal DC development.....	41
3.9	Genetic deletion of <i>Ch25h</i> leads to a deficiency of pulmonary cDC2 during homeostasis.....	44
3.10	Fibroblasts produce key enzymes related to GPR183 ligand and regulate cDC2s via TSLP-CRLF2 (TSLPR)	45
4	Discussion.....	50
4.1	Unambiguous discrimination of <i>bona fide</i> cDCs and the expression pattern of <i>Gpr183</i>	51
4.2	GPR183 regulates maintenance of cDC2s and their subsets intrinsically	52
4.3	Decrease in pulmonary cDC2 abundance is due to impaired proliferation and apoptosis	53

4.4 Decreased pulmonary cDC2s does not affect influx of pre-cDC2s in the lung.	54
4.5 Decreased pulmonary cDC2s influence the migratory cDC2s in the draining LN	54
4.6 Fibroblasts are the main producers of GPR183 ligand in the lung and GPR183 – 7 α ,25-OHC axis is important to keep cDC2s maintenance.	55
4.7 Niche factor, TSLP produced by adventitial fibroblasts is critical to keep pulmonary cDC2s maintenance.	56
5 Acknowledgements	60
6 Reference.....	62

Abstract

G protein-coupled receptor 183 (GPR183) is a chemotactic receptor, highly expressed by immune cells. Upon activation by its ligand, $7\alpha,25$ -dihydroxycholesterol ($7\alpha,25$ -OHC), GPR183 activates downstream signals inducing a wide range of functional responses, including inflammation, cell migration, and proliferation. Earlier work has shown that GPR183 is critical for the correct positioning of splenic dendritic cells (DCs) and the initiation of subsequent DC dependent adaptive immune responses. Whether GPR183 has a role in the localization and function of DCs in the murine lung has not been investigated.

To understand its role in lung DC homeostasis and development we analyzed the abundance and phenotype of lung dendritic and stromal cell populations in WT and GPR183 KO animals using high dimensional flow cytometry alongside transcriptomic, functional and spatial analysis.

We found that the absence of GPR183 resulted in a specific decrease of the resident pulmonary cDC2 population due to impaired *in situ* proliferation and increased apoptosis. In contrast, DC development was not affected by GPR183 ablation. Furthermore, analysis of the CH25H deficient mice revealed that CH25H dependent production of $7\alpha,25$ -OHC is crucial for pulmonary cDC2 homeostasis. Adventitial fibroblasts are the major producer of $7\alpha,25$ -OHC in the lung. Therefore we assessed the subtissular location of pulmonary cDC2 in the lung. This analysis revealed that cDC2 closely associate, in a GPR183 dependent manner, with adventitial fibroblasts. Next using single-cell transcriptomic data and cellular interaction modeling, we identified the thymic stromal lymphopoietin (TSLP) – TSLP receptor (TSLPR) axis as a possible

candidate promoting cDC2 survival in a GPR183 dependent manner. Accordingly, DC-specific TSLPR KO mice had decreased pulmonary cDC2s numbers.

Collectively these findings demonstrate that GPR183 plays an intrinsic role in cDC2 maintenance and reveals GPR183 as a crucial regulator of peripheral organ resident DCs homeostasis and subtissular location. What is more, GPR183 – 7 α ,25-OHC acts as a guiding axis for pulmonary cDC2 localizing in their supporting subtissular niche where cDC2s have access to pro-survival factors such as TSLP – TSLPR instructed by fibroblasts.

Keywords: Mononuclear phagocytes, Dendritic cells, Adventitial fibroblasts, G Protein-coupled receptor 183, Conventional dendritic cells, Tissue niche, TSLP

List of abbreviations

abbreviation	Full name
BM	bone marrow
EDTA	ethylenediaminetetraacetic acid
7α, 25-OHC	7 α , 25-dihydroxycholesterol
AM	alveolar macrophage
BATF3	basic leucine zipper ATF-like transcriptional factor 3
cDC	conventional dendritic cell
CDP	common DC progenitor
CH25H	cholesterol 25-Hydroxylase
CRLF2	cytokine receptor-like factor 2
CYP7B1	cytochrome P450, family 7, subfamily b, polypeptide 1
DC	dendritic cell
DDS	dextran sulfate sodium
EBI2	epstein-barr virus-induced gene 2
ERK1/2	extracellular signal regulated kinase 1/2
FLT3L	fms-related tyrosine kinase 3 ligand
FSC	forward scatter
FVD	fixable viability dye
GC	germinal center
GPR183	G-protein coupled receptor 183
GRC	genetic resources center

HDM	house dust mite
HE	hematoxylin and eosin
HSD3B7	hydroxy-delta-5-steroid dehydrogenase, 3 beta and steroid delta-isomerase 7
ID2	inhibitor of DNA binding 2
IFN	interferon
ILC3s	Group 3 innate lymphoid cells
inf-DC	inflammatory dendritic cell
IRF4	interferon regulatory factor 4
IRF8	interferon regulatory factor 8
KO	knockout
LIN	lineage
M-cDC	migratory cDC
MCs	monocyte derived cells
MDP	macrophage and DC progenitors
MHC II	major histocompatibility complex class 2
MPS	mononuclear phagocyte system
PCLS	precision-cut mouse lung slice
PCR	polymerase chain reaction
pDC	plasmacytoid dendritic cell
RBC	red blood cell
RT	room temperature
SPF	specific pathogen free

SRE	serum response element
SSC	side scatter
TF	transcriptional factor
Tfh	T follicular helper
TLR3	Toll-like receptor 3
TSLP	thymic stromal lymphopoietin
TSLPR	thymic stromal lymphopoietin receptor
UMAP	uniform manifold approximation and projection
WT	wildtype
ZBTB46	zinc finger and btb domain-containing protein 46

1 Introduction

1.1 Dendritic cells (DCs) link innate and adaptive immunity

Myeloid and lymphoid lineages are the two major branches of the immune system. The lymphoid compartment is responsible for adaptive immunity induced mainly by T and B cells, while the myeloid compartment, comprising mononuclear and polymorphonuclear cells, such as macrophage, monocyte, and dendritic cells, participates mostly in innate immunity. As a crucial part of mononuclear phagocytes and innate immunity, DCs are specialized in antigen capturing and processing, and able to migrate to lymphoid tissues in a CCR7-dependent manner^[1, 2] to present phagocytosed antigens to naive T cells initiating an adaptive immune response^[3]. Thus, DCs are the bridge that links innate and adaptive immunity and play a critical role in orchestrating the immune response.

DCs with distinct morphology features were first described in lymphoid tissues by Steinman RM and Cohn ZA in 1973^[4]. They are present in lymphoid and non-lymphoid organs, as well as circulation of the body, where they form the critical part of immune systems in human and mice. In recent years, our understanding of DC subsets, their development, and the functional specialization in different tissues within mouse and human has accumulated greatly due to advent of multi-parameter flow cytometry, mass cytometry and RNA sequencing.

1.2 Phenotypic diversity and functional division within DCs networks

Considerable effort has been made on the accurate identification and classification of DCs. Based on their ontogeny, transcriptional factor (TF) and functional specialization,

DCs network can be classified into three main groups, namely the plasmacytoid DCs (pDCs), the conventional DCs (cDCs), and the inflammatory DCs (inf-DCs).

1.2.1 Phenotype and function of pDCs

pDCs and cDCs can be found both in lymphoid and non-lymphoid organs in the steady state. pDCs with round morphology can be identified by two common markers, Siglech and B220^[5]. pDCs have varied lifespan between mouse strains and are continuously produced in the bone marrow (BM) and migrate as mature cells into the periphery^[6]. The development of pDC is strictly dependent on the FLT3L and the lineage specific TF TCF4^[7, 8]. pDCs are critical in antiviral immune responses since they are capable of massive and rapid production of broad spectrum of interferons (IFNs) during viral infections^[9].

1.2.2 Phenotype and function of cDCs

Compared to pDCs, cDCs with stellate morphology are more phenotypically and functionally heterogeneous. The expression of MHCII and CD11c has been extensively used to identify cDCs in human and mouse. CD26 was added as an additional marker to well define cDC population, since it is highly expressed on all cDCs across multiple tissues^[10]. The TF Zinc finger and btb domain containing 46 (ZBTB46) is selectively expressed by cDCs and their committed progenitors^[11, 12]. Its expression can be used to further discriminate from pDCs. Functionally, all cDCs share a common feature, namely to present antigen to T and B cells in an MHC class I and II restricted manner. cDCs have been divided into two main subsets, termed cDC1 and cDC2^[13], on the basis of a set of surface markers, ontogeny, transcriptional requirements, and functional specialization.

1.2.2.1 Phenotype and function of cDC1s

cDC1s have been well characterized and are a relatively homogeneous population, which can be found in all murine lymphoid as well as non-lymphoid tissues. Within these tissues, cDC1s are identified by the expression of CD8, CD103, CD24 and XCR1^[14]. Importantly, the expression of XCR1 on cDC1s is broadly conserved across species^[10]. Genetic and functional studies have revealed that interferon regulatory factor 8 (IRF8)^[15, 16], basic leucine zipper ATF-like transcriptional factor 3 (BATF3)^[17, 18] and inhibitor of DNA binding 2 (ID2)^[15, 19]-dependent cDC1s are functionally specialized in cross-presentation of antigens to CD8⁺ T cells via CLEC9A, in response to necrotic cells antigens^[20], and via WDFY4, in response to viral or tumor antigens^[21]. In addition, cDC1s are capable to secretion of IL-12 to facilitate polarization into the Th1 subset^[22] and secretion of INF- γ in response to stimulation via Toll-like receptor 3 (TLR3)^[23], emphasizing its role in acting against intracellular pathogens.

1.2.2.2 Phenotypic diversity and functional division of cDC2s

In contrast, cDC2s which also populate both lymphoid and non-lymphoid tissues, are less-well understood and contain heterogeneous populations. They can be distinguished from cDC1s by their preferential expression of the surface markers CD4, CD11b, and CD172 α ^[14]. The development and maintenance of cDC2s depend on TF IRF4^[24]. cDC2s are functionally specialized in the presentation of antigen to CD4⁺ T cells. IL-10 and IL-33 are produced by cDC2s to favor polarization towards Th2 responses^[25], and IL-6 is produced to favor polarization towards Th17 responses^[26], particularly within barrier organs such as skin, intestine and lung, which emphasizes their importance during immune responses to extracellular pathogens.

Importantly, additional subsets can be delineated within the cDC2s branch across tissues depending on the expression of certain TF such as NOTCH2, KLF4 and T-bet. This indicates their multiple functions due to differences in TF expression, location and cytokine production. Murphy and colleagues dissect cDC2 heterogeneity showing a KLF4-dependent cDC2 subset across several tissues, including LN, lung, spleen and intestine. ESAM^{hi} cDC2 in the spleen and CD103⁺CD11b⁺ cDC2 in intestine are dependent on the expression of NOTCH2^[27, 28]. KLF4 guides a transcriptional program necessary for Th2 cell immunity during house dust mite (HDM) challenge, and *S. mansoni* infection^[25, 29, 30]. IL-23 production by NOTCH2-dependent cDC2s in intestine is required for modulating Th17 differentiation and function^[28, 31]. In addition, NOTCH2 dependent cDC2s play an important role in promoting Tfh and germinal center (GC) B cell formation^[32].

Both of the above mentioned TFs used to delineate cDC2s heterogeneity were mostly explored in mice. However, their human equivalents remain largely elusive. Recently, Rudensky group^[33] described two distinct subsets of cDC2s based on the expression of T-bet, which is conserved in mice and humans across tissues, showing that ROR γ t⁺T-bet⁻ cDC2s (cDC2B) have a more pro-inflammatory profile, while T-bet⁺ cDC2s (cDC2A) are involved in tissue repair. What's more, the surface marker CD301b/Mgl2 is exclusively expressed by T-bet⁻ cDC2s (cDC2B). CD301b⁺ DCs, a major subset of cDC2s in mouse skin, have been also studied in the lung and LN. Multiple studies from the Kumamoto group showed that CD301b⁺ DCs are able to dictate CD4⁺ T cell fate, drive Th2 responses, and suppress T follicular helper cells^[34, 35].

1.2.3 Phenotype and function of inf-DCs

Inf-DCs are the most controversial of the three populations. Together with CD26, CD64 and Mar-1 were applied to separate inf-DCs from cDCs and monocyte derived cells (MCs). Inf-DCs are derived from preDC under inflammatory conditions or infections^[36]. *Bona fide* inf-DCs are able to migrate to LN and prime CD4 and CD8 T cells.

1.3 Ontogeny of DCs: from BM progenitors to DC subsets in tissues

DCs arise from a hematopoietic lineage which is distinct from other leukocytes, establishing DCs as a unique hematopoietic branch. Sequential stages of DCs' development from distinct BM progenitors have been defined during the past decades. Phenotypic markers, as well as expressed TFs, and activated signaling pathways to distinguish cDC progenitors at each stage, have been well-elucidated in numerous research (**Fig. 1-1**)^[37].

Evidence from adoptive transfer studies of irradiated animals showed that most DCs arise from a specific hematopoietic progenitor that undergoes cascades of developmental programs to terminally differentiate in peripheral tissues. Macrophage and DC progenitors (MDP) are bi-potent progenitors giving rise to both monocytes and DC progeny in an IRF8-dependent manner^[38]. MDP further differentiate into common DC progenitor (CDP), which has been identified as a clonogenic progenitor that has lost the potential to differentiate into monocytes or macrophages, and generate exclusively and efficiently to pDCs and cDCs^[39, 40]. pDCs terminally differentiate in the BM due to up regulation of IRF8 and TCF4, and downregulation of ID2 and ZBTB46^[41], and reach peripheral organs as fully developed cells via blood stream. Pre-cDCs originating from CDP contain cDC subset-committed progenitors, namely pre-cDC1 and pre-cDC2^[42],

which exit the BM and migrate through blood to seed in peripheral tissues and give rise to mature cDC1 and cDC2 respectively according to peripheral cues and action of TFs. IRF8, BATF3 and ID2 drive the development and terminal differentiation of cDC1 lineage^[38, 43]. On the other hand, IRF4, KLF4 and NOTCH2 drive the development of cDC2s^[24, 44]. In addition to the activity of different TFs, the main cytokine required for DCs' development is FLT3L^[15, 45, 46].

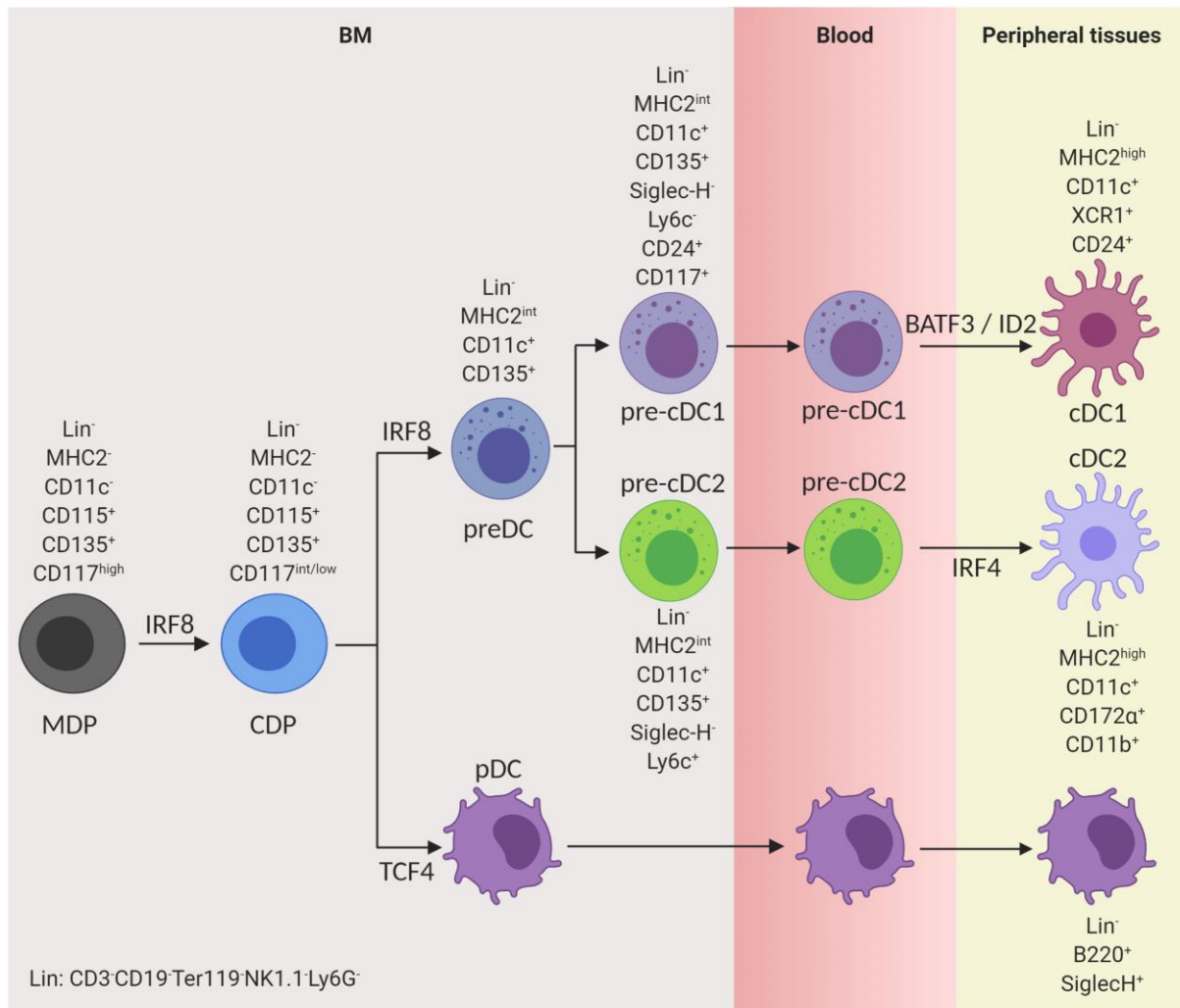


Figure 1-1. Developmental scheme of mouse DC development from BM early progenitors and lineage-committed progenitors (adapted from^[47-49]). DCs including pDC and cDC develop from BM in a stepwise manner. CDP arises from MDP, a step regulated by the TF IRF8. CDP

further generates preDC and mature pDC, depending on IRF8 and TCF4 respectively. pDC seeds in peripheral tissues via blood stream. preDC splits into cDC1 committed pre-cDC1 and cDC2 committed pre-cDC2. These pre-cDCs leave BM into blood stream and seed into tissues where they get tissue specific signals to become cDC1s and cDC2s. The development of cDC1s depends on BATF3 and ID2, while cDC2s require IRF4.

1.4 The mononuclear phagocyte system (MPS) strategically locates within different sites of the lung

The lung is constantly exposed to the external environment and faces particular immunological challenges, such as a wide variety of microbes, dusts and pollutants. Therefore, the lung contains a sophisticated network of immune cells which maintain homeostasis, especially the MPS networks (**Fig. 1-2**) comprising macrophages, monocytes and DCs. Alveolar macrophages (AMs) sit within the alveolar space and can quickly phagocytose pathogenic antigens, scavenge damaged cells and promote tissue repair^[50]. Both cDC1s and cDC2s are professional antigen presentation cells, but they locate in different sites of the lung. cDC1s were detected around the airways and in subpleural region, whereas cDC2s resided primarily in parenchyma^[51]. However, the mechanism by which they strategically locate and migrate is poorly understood and it is not clear if there is a niche factor which educates DCs to maintain themselves in lung tissue.

GPR183 has been identified as a guiding factor in spleen as it regulates the localization and function of DCs^[52]. The lung is one of the organs that express high level of *Gpr183*^[53]. Furthermore, AMs was reported to express CH25H which is critical enzyme

to generate GPR183 ligand^[54]. To date, the role of GPR183 has been mainly studied in lymphoid tissues. Its role in barrier tissues, especially the lung which shows high level of GPR183, remains insufficiently studied.

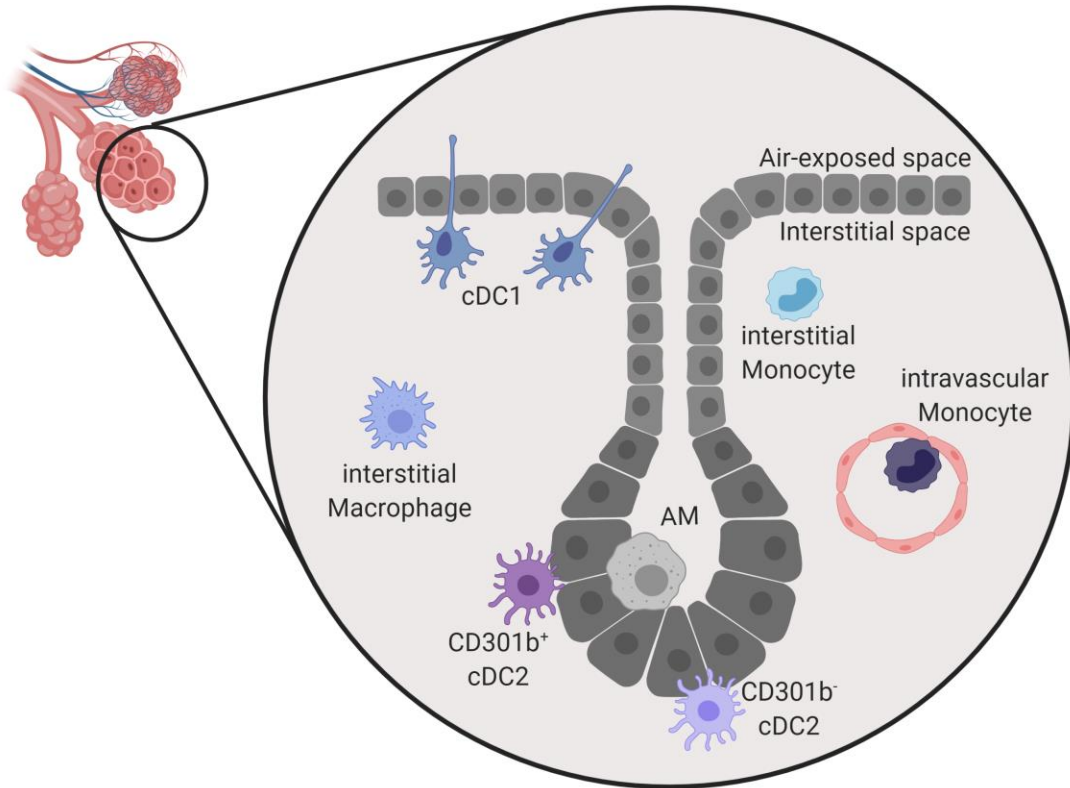


Figure 1-2. Subsets of MPS within lung tissue in steady state. Subsets of MPS reside in different locations of the lung in order to handle and remove the various threats present in inhaled air, such as viruses and bacteria. AM is located in alveolar space and able to quickly remove inhaled pathogens. cDC1 sits underneath the epithelial cells where they can extend their dendrites between epithelial cells to airway lumen, whereas subsets of cDC2 resides in parenchyma. The lung interstitium contains interstitial macrophage, monocyte and DC^[55].

1.5 GPR183 and its ligand 7 α ,25-OHC

G protein-coupled receptor 183 (GPR183), also known as epstein-barr virus-induced gene 2 (EBI2), is a Gai protein coupled receptor. It is a chemotactic receptor which is

highly expressed in many immune cells, such as T cells, B cells and DCs^[52, 56, 57]. The physiological and most potent ligand for GPR183 is 7 α ,25-dihydroxycholesterol (7 α ,25-OHC)^[58, 59], which is synthesized from cholesterol via sequential hydroxylation by the enzyme 25-hydroxylase (CH25H) and cytochrome P450 family 7 subfamily b polypeptide 1 (CYP7B1). Hydroxy-delta-5-steroid dehydrogenase, 3 beta- and steroid delta-isomerase 7 (HSD3B7) further metabolizes 7 α ,25-OHC into 7 α ,25-HCO that lacks ligand activity (**Fig. 1-3**). By binding to its ligand, GPR183 triggers downstream signals inducing calcium mobilization, activation of extracellular signal regulated kinase (ERK1/2), p38, as well as serum response element (SRE), and all of these lead to a wide range of functional immune responses, such as inflammation, proliferation and migration (**Table 1-3**). Noteworthy is the fact that β -arrestin is recruited to induce GPR183 internalization after engagement by its ligand^[60, 61]. There are currently two GPR183 competitive antagonists, NIBR189 and GSK682753A^[62, 63].

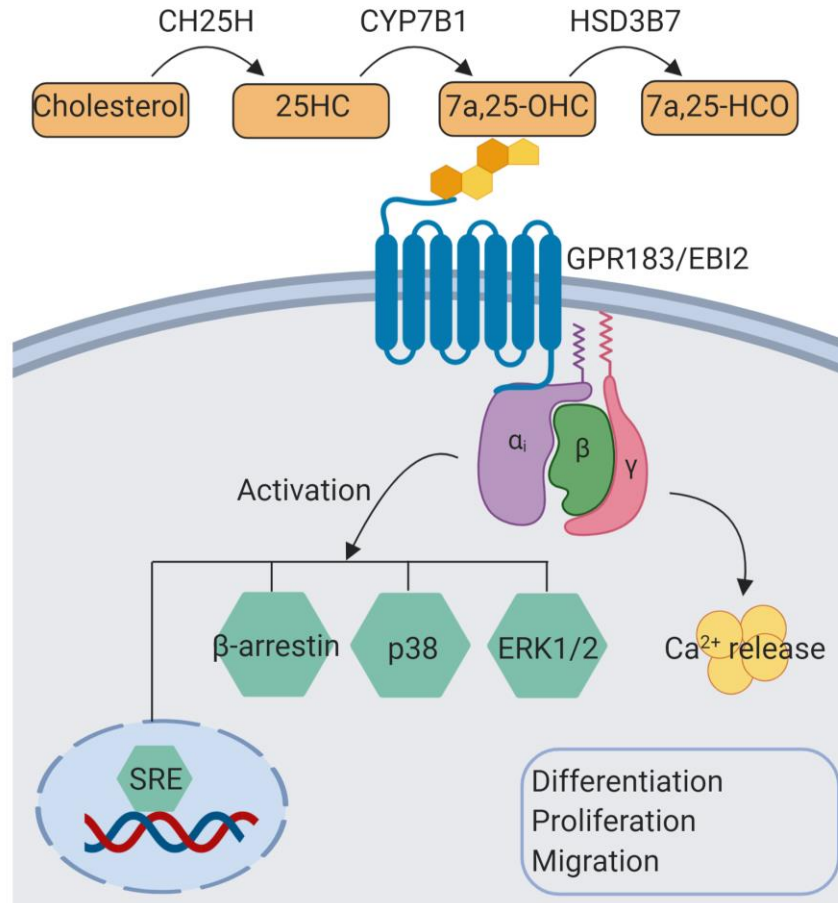


Figure 1-3. GPR183 – 7 α ,25-OHC axis signaling pathways. (adapted from^[64]) GPR183 signals through G α protein, leading to activation of SRE, ERK1/2, p38, β -arrestin and calcium release. The most potent ligand for GPR183 is 7 α ,25-OHC which is generate from cholesterol by sequential hydroxylation with CH25H and CYP7B1, and degraded by HSD3B7. Downstream activation of GPR183 by 7 α ,25-OHC induces a wide range of functional responses, such as differentiation, proliferation, and immune regulation.

1.6 Immune regulation of GPR183 – oxysterol (7 α ,25-OHC) axis

In recent years, emerging evidence has revealed that functional dysregulation of GPR183 or the ligand synthesis contributes to inflammation, cell migration, proliferation and autoimmune or metabolic diseases.

It was first reported that GPR183 played a critical role in B cell migration^[65, 66] by showing that GPR183 expression by activated B cells facilitate their migration to the outer follicle of the murine spleen. After the identification of the endogenous ligand, 7 α ,25-OHC in 2011^[58, 59], numerous subsequent studies using genetic KO mice support the role of GPR183 in migration of various cell populations, including T cells, astrocytes, eosinophils, monocytes, and DCs^[52, 67-69] (**Table 1–1**). Absence of GPR183 failed to guide the positioning of CD4⁺ T cells to the interface of the follicle and T cell zone, where they had access to T follicular helper (Tfh) cells differentiation signals delivered by CD25^{hi}ICOSL^{hi} cDCs^[70]. In addition, GPR183 deficient mice showed fewer DCs and were defective in maintenance of cDC2s, correct homing of splenic DCs, and initiation of T cells responses^[52]. Blocking GPR183 *in vivo* with its antagonist NIBR189 mimicked the phenotype of GPR183 deficient mice^[71]. Genetic deficiency in *Ch25h* or *Cyp7b1* had been shown to cause abnormal B cells positioning in LN^[72] and also caused decreased number of DC in spleen^[71] due to reduced content of 7 α ,25-OHC from stromal cells.

The biological effects of GPR183 have been largely credited to the migration of immune cells within lymphoid tissues. There are also evidences linking GPR183 with inflammation, tissue homeostasis and human diseases. Furthermore, GPR183 has been listed as a risk factor for inflammatory bowel disease. Increased mRNA levels of *Gpr183* and ligand synthesizing enzymes (CH25H, CYP7B1) have been found in inflamed colon and dextran sulfate sodium (DDS) induced colitis^[56]. GPR183⁺ Group 3 innate lymphoid cells (ILC3s) sense localized oxysterol provided by fibroblastic stromal cells and are critical for tissue integrity in the intestine^[73].

Table1-1. Immune functions of GPR183 in different cell populations

cell population	function of GPR183	tissue	reference
T cells (Tfh, Th17)	migration, differentiation	spleen, LN, brain	[67, 70, 74, 75]
B cells	migration, proliferation	spleen, LN	[59, 65, 66, 76]
macrophages	infection, survival	cell line	[77]
DCs	migration, maintenance	spleen, LN	[52, 71]
ILC3s	migration, inflammation	intestine	[56]
eosinophils	migration	lung	[69]

2 Materials and methods

2.1 Materials

2.1.1 Mice

Gpr183^{-/-}, *Gpr183*^{fl/EGFP} and *Ch25h*^{-/-} were kindly provided by Prof. Dr. Alexander Pfeifer. CD45.1 and *Zbtb46-cre* were purchased from Jackson lab. To generate DC conditional depletion of *Gpr183*, *Gpr183*^{fl/fl} mice were crossed with *Zbtb46-cre* mice. To generate DC conditional depletion of *Tslpr*, *Tslpr*^{fl/fl} mice were crossed with *CD11c-cre* mice in Prof. Steven F. Ziegler lab.

Mice were bred and housed in a specific pathogen-free (SPF) condition in Genetic Resources Center (GRC) of the Life & Medical Sciences (LIMES) Institute, University of Bonn, Germany. 8-15weeks old mice were used in all experiment. All animal experiments were carried out according to protocols (2019.A256- Untersuchung der Rolle von GPR183 für die Entwicklung und Funktion von lungenresidenten dendritischen Zellen, 2017.A347- Einfluss der Gedächtnissfunktion des angeborenen Immunsystems auf die Entwicklung und schwere von akuter und chronischer Entzündung in der Lunge) approved by Landesamt für Natur, Umwelt und Verbraucherschutz Nordrhein Westfalen.

2.1.2 Consumables

Table 2-1, Consumables

Product	company
1.5 ml, 2 ml reaction tubes	Eppendorf
15 ml, 50 ml tubes	Greiner bio-one

Cell culture plates (6-well, 12-well, 24-well flat bottom)	Greiner bio-one
Disposal autoclave bags	Roth
Flow cytometry tubes	Sarstedt
Serological pipettes (10ml, 25ml)	Greiner bio-one
Sterican needles (1.1x50mm, 19G x 2")	B/Braun
Sterican needles (0.55x25mm, 24G x 1")	B/Braun
Syringes Inject® (2ml, 5ml)	B/Braun
Aluminium foil	Carl Roth
Parafilm	Carl Roth
PCR tubes	VWR
EASYstrainer™, 70 µm	Greiner Bio-One
Gloves	SemperGuard
FACS tube	SARSTEDT

2.1.3 Equipment

Table 2-2, Equipment

Equipment	Company
Autoclave	H+P Varioklav Dampfsterilisator EP-2
Incubator	Memmert
Cell culture incubator	Binder
Balances	Kern & Sohn
Cell counting chamber	La Fontaine via Labotec - improved neubauer
Centrifuges	Eppendorf

Confocal Microscope	Zeiss LSM880
Electro pipet	BRAND
Flow Cytometer (LSRII)	BD bioscience
Flow Cytometer (FACSymphony A5)	BD bioscience
Flow Cytometry sorter (FACSAria III)	BD bioscience
Fluorescence microscopy	KEYENCE
Microwave	Panasonic NN-E201WM
PCR machine	Biometra
Real Time PCR machine	Bio-Rad
Thermo block	Eppendorf
Vortex	Vortex Genie2
Water bath	Julabo SW22

2.1.4 Reagents and kits

Table 2-3, Reagents and kits

Reagent	Company
miRNeasy Micro Kit	Qiagen
QuantiTect Reverse Transcription Kit	Qiagen
Albumin Bovine Fraction V, pH 7.0 (BSA)	SERVA
Ammonium chloride (NH ₄ Cl)	Carl Roth GmbH
Collagenase from Clostridium histolyticum	Sigma-Aldrich
Deoxyribonuclease I from bovine pancreas (DNase I)	Sigma-Aldrich
DRAQ7™	BioLegend

HBSS	PAN-Biotech
Precision Count Beads™	BioLegend
ROTI®Cell 10x DPBS	Carl Roth GmbH
Sodium hydrogen carbonate (NaHCO ₃)	Carl Roth GmbH
UltraPure™ EDTA	Invitrogen
Annexin V	eBioscience
Annexin V Binding Buffer (10x)	eBioscience
Collagenase Type IV	Sigma-Aldrich
Fixation/ Perm Diluent	eBioscience
Fixation/ Permeabilization Concentrate	eBioscience
Fixable Viability Dye eFluor™ 660	eBioscience
Fixable Viability Dye eFluor™ 780	eBioscience
Permeabilization Buffer (10x)	eBioscience
Recombinant Murine Flt3-Ligand	PeptoTech
Agarose(Low Melting Point)	Promega
GoTaq qPCR master mix	Promega
GeneRuler 1kb Plus DNA Ladder	Thermo Fisher Scientific
2-Propanol >99.5%	AppliChem
Ethanol	Carl Roth
Ethanol absolute for molecular biology	AppliChem
Ethylenediaminetetraacetic acid (EDTA)	Thermo Fisher Scientific
RPMI-1640	PAN Biotech
Penicillin-Streptomycin	Thermo Fisher Scientific

Tween-20	SIGMA
TruStain fcXTM (anti-mouse CD16/32) (Clone: 93)	Biolegend
RTU Animal-Free Block and Diluent	VECTOR

2.1.5 Buffers

Table 2-4, Buffers

Buffer	Content
Complete RPMI 1640	RPMI Medium 10% FCS 1% Penicillin-Streptomycin
0.5M EDTA	186.1 g EDTA approx. 20 g NaOH 1L H ₂ O pH 8.0
Histology washing buffer	0.01% Tween-20 in 1 X PBS
Blood collection buffer	500 ml 1 X PBS 1.86 g EDTA
Red blood cell lysis buffer	8.32g NH ₄ CL 0.84g NaHCO ₃ 0.043g EDTA 1L H ₂ O
Tail lysis buffer	0.1 M Tris 5 mM EDTA, pH 8,0 0,2 % SDS 0.2 M NaCl 0,1 mg/ml Proteinase K
FACS buffer	1 X PBS 0.5% BSA 2mM EDTA
4% PFA	40g PFA 1L 1 X PBS pH 7.4

2.1.6 Antibodies used for FACS and histology staining

Table 2-5, Antibodies used for FACS and histology staining

Antibodies	Fluorophore	clone	company	Titration
CD115	PE/Dazzle™594	AFS98	BioLegend	1:100
CD117	PE-Cy7	2B8	BioLegend	1:100
CD11b	BV421	M1/70	BioLegend	1:200
CD11c	PerCp-Cy55	N418	BioLegend	1:100
CD11c	BV421	N418	BioLegend	1:100
CD135	PE	A2F10	eBioscience	1:100
CD172α	PE/Dazzle™594	P84	BioLegend	1:200
CD19	APC/Cy7	6D5	BioLegend	1:200
CD24	PE	M1/69	BioLegend	1:500
CD3	APC/Cy7	145-2C11	BioLegend	1:200
CD301b	APC	URA-1	BioLegend	1:200
CD45	FITC	I3/2.3	BioLegend	1:200
CD45R	APC	RA3-6B2	BioLegend	1:100
CD45R	APC/Cy7	RA3-6B2	BioLegend	1:200
CD64	PE-Cy7	X54-5/7.1	BioLegend	1:100
F4/80	BV786	BM8	BioLegend	1:300
LY6C	BV605	HK1.4	BioLegend	1:200
Ly6G	APC/Cy7	1A8	BioLegend	1:200
MHC2	BV510	M5/114.15.2	BioLegend	1:200
NK-1.1	APC/Cy7	PK136	BioLegend	1:200
Siglec F	PE-CF594	E50-2440	BD Biosciences	1:400

Siglec H	PerCp-Cy55	551	BioLegend	1:200
TER-119	APC/Cy7	TER-119	BioLegend	1:200
XCR1	APC	ZET	BioLegend	1:200
Annexin v	PE-Cy7		eBioscience	1:50
Caspase3	FITC	C92-605	BD bioscience	1:50
Ki67	APC	SoIA15	eBioscience	1:200
ERK1/2	PE-Cy7	6B8B69	BioLegend	1:50
pSTAT3	BV421	13A3-1	Biolegend	1:50
pSTAT5	PE	SRBCZX	Invitrogen	1:50
CD88	PE	20/76	Biolegend	1:100
PDGFR α	APC	APA5	BioLegend	1:200
CD172 α	APC	P84	eBioscience	1:100
CD45	BUV395	30-F11	BD bioscience	1:200
CD45	BV785	30-F11	Biolegend	1:200
XCR1	BV650	ZET	BioLegend	1:200
CD172 α	PE-Cy7	P84	Biolegend	1:200
Siglec-F	BUV395	E50-2440	BD bioscience	1:400
CD301b	PE/Dazzle 594	URA-1	BioLegend	1:200
CD45	BV421	30-F11	BioLegend	1:200
CD11b	AlexaFluor®700	M1/70	BioLegend	1:200
Ly6G	APC	1A8	BioLegend	1:400

2.2 Methods

2.2.1 Isolation of cells from blood, BM and lung

Blood was collected from heart after cervical dislocation. BM cells were harvested by flushing femurs and tibias with PBS. Lungs were removed from mice and minced with scissors. Minced lungs were digested in HBSS buffer supplemented with 0.1mg/ml collagenase type IV and 50ug/ml DNase I, for 30min in a 37°C incubator. After digestion, homogenize cell suspension with 19G syringe and needle. Cells were meshed through a 70 um cell strainer. After washing with FACS buffer, cells are ready to stain.

2.2.2 PFA-fixed, paraffin embedded lung for histology staining

The mice were anaesthetized with combination of ketamine and xalyxin. The lungs were perfused with 10ml PBS and 10ml 4 % PFA sequentially. The lung lobes were collected and immersion fixed with 4 % PFA O/N at 4°C, followed by 70% ethanol incubation at 4°C until needed. Dehydration was carried out by immersing lung lobes in series of ethanol solution in an automated tissue processor (Leica). Clearing and wax infiltration were followed in xylene solution and histology wax in the same tissue processor. Afterwards, the lung lobes were properly orientated and embedded in wax-filled mold and cassette using an embedding center (Leica). 4 µm sections were mounted onto glass slides after cutting with Leica RM 2255 Microtome.

2.2.3 Hematoxylin and eosin (HE) staining

The lung paraffin sections were placed in xylene twice, each for 5 minutes. The lung sections were then rehydrated with 100 %, 95 % and 70 % ethanol solution, each for 5 minutes and afterwards rinsed with distilled water for 5 minutes. After drying shortly,

lung sections were incubated with hematoxylin for 5 minutes to stain the nuclei in blue color, followed by washing under running tap water until water becoming clear. The lung sections were then incubated with 0.5% eosin for around 2 minutes to stain the extracellular matrix in pink color, followed by washing under running tap water until water becoming clear. To dehydrate the sections, the lung sections were rinsed with an ascending ethanol grades (70 %, 95% and 100 % ethanol) for 2 minutes each. After clearing in xylene twice, each for 3 minutes, the lung slides were mounted with VectaMount™ and analyzed under a light microscope.

2.2.4 Alcian blue and nuclear fast red staining

The lung sections were dewaxed and cleared as described above. After washing, the slides were incubated in alcian blue solution to stain the acid mucosubstances, followed by washing under running tap water until water becoming clear. The nuclei of the lung sections were then stained with nuclear fast red aluminum sulfate solution for 10 minutes, followed by washing under running tap water until water becoming clear. To dehydrate the sections, the lung sections were rinsed with an ascending ethanol grades (70 %, 95% and 100 % ethanol) for 2 minutes each. After clearing in xylene twice, each for 3 minutes, the lung slides were mounted with VectaMount™ and analyzed under a light microscope (Biorevo).

2.2.5 Quantitative real time (RT)-PCR

Endothelial cells, epithelial cells, stromal cells and total myeloid cells were sorted into TRIzol reagent. RNA was extracted using miRNeasy Micro Kit. RNA was reverse transcribed by QuantiTect Reverse Transcription Kit. Genes' expression of *Gpr183*, *Ch25h*, *Cyp7b1* and *Hsd3b7* were analyzed using GoTaq qPCR master mix and Bio-

Rad CFX96 Real-Time PCR Detection System. Primer sequences are listed in Table 2-6. Expression of each gene was calculated relative to the housekeeping genes PPIA. Relative expression levels (fold changes) were determined by $\Delta\Delta C_t$.

Table 2-6. Primer sequences used for quantitative RT-PCT

Gene	Forward primer	Reverse primer
<i>Gpr183</i>	ATAGACCGCTTCTTCGCTGT	AGACCAGAATCCAGACGGAC
<i>Ch25h</i>	GTGCATCACCAGAACTCGTC	AAGTCATAGCCCGAGTGGTC
<i>Cyp7b1</i>	TCTGGGCCTCTCTAGCAAAC	AATAGTGCTTTCCAGGCAGAC
<i>Hsd3b7</i>	CAGTCCAGGACACAACCTCC	CTGCCATGCCCGAGCTGTA

2.2.6 Immunofluorescence microscopy

Lung preparation Precision-cut mouse lung slice (PCLS) was applied to visualize pulmonary cDC2s. Detailed protocol was referenced to publication^[51]. Briefly, mouse was euthanized and pinned on the dissection board. Inferior vena was sniped to drain the blood away from lung. Polyethylene tubing was used to inject 0.8 ml pre-warmed 2% low melting agarose. The trachea was tightened and agarose inflated lung was transferred to cold PBS for at least 30min before going to section.

Lung section Each lobe was separated and kept in cold PBS. The right superior lobe was transferred to a 12-well plate filled with 4% pre-warmed low melting agarose. The interior part of the lung was face down in the well. Wait until agarose was solidified on ice. Load agarose embedded lung into the Vibratome slicer, align blade and set thickness (200 μm), speed (0.3) and oscillation (0.85) according to manufacturer. The 7th –10th slices were taken for staining.

Staining 200 μm thick sections of the fresh lung were first treated with a blocking buffer for 20 min on ice. Sections were then incubated with primary antibodies (CD88,

CD172 α , CD11c, PAGFR α) O/N in the dark, followed by 1 h incubation with secondary antibodies (Donkey anti-Goat IgG, Alexa Fluor 488) at RT. Sections were sealed in PBS with nail polish. Images were captured in Zeiss LSM880 confocal microscope with 20X or oil objective. All images were quantified with ImageJ or Imaris.

2.2.7 Flow cytometry

Surface staining: Cell from single-cell lung suspensions were blocked with CD16/32 for 10 min before incubating with antibody cocktails for 30 min at 4°C in dark. After washing with FACS buffer, cells were re-suspended by 2 ml RBC lysis buffer and incubated for 4 min at room temperature (RT). Dead cells were labeled by adding Draq7 after washing the lysis buffer. Cells were analyzed on a BD FACS Canto II or Symphony flow cytometer. Data were analyzed in FlowJo V10. For determination of absolute cell numbers, 5 μ l beads were used according to manufacturer's instructions. Cell population number per μ l = (number of cells in specific gate X number of beads in 5 μ l)/(number of beads in specific gating X total volume of cell suspension)

Intra-cellular staining: Intracellular staining was performed using the Intracellular Staining Kit (BD Biosciences). Briefly, before blocking with CD16/32, cells were stained with fixable viability dye (FVD)780 for 10 min at 4°C in dark, followed by normal surface staining. After washing, cell were fixed and permeabilized with BD cytofix/cytoperm 30min at 4°C in dark. Cells were then ready to be measured after incubated with intracellular antibodies (caspase3) for 30min at 4°C in dark.

Intra-nuclear staining: Similar with intra-cellular staining, cells were incubated with CD16/32, FVD780 and surface antibody mix sequentially. Then fixation and permeabilization were performed using combination of fixation/permeabilization

concentrate and dilute for 30 min, at RT. Followed by intra-nuclear antibody (Ki67) staining for 30 min at RT in dark.

Apoptosis staining: To stain apoptosis cells, caspase3 was performed with intracellular staining mentioned above, and annexinV were measured according to the manufacturer's instructions. Briefly, after surface staining, cells were incubate with annexin V for 15 min at RT, followed by RBC lysis, cells are ready to be measured.

2.2.8 Culture of BM derived DC

BM cells were flushed from WT and *Gpr183* KO mice and lysed by red blood cells lysis buffer. Cells were counted and re-suspend in 1.5 million cells per ml RPMI medium supplemented with L-glutamine, penicillin/streptomycin, non-essential amino acids, β -mercaptoethanol and 10% FCS. Seed 3 ml cells in 6-well plate and add 100 ng FLT3L per well. DCs were measured at day7.

2.2.9 Generation of BM chimeras

CD45.1 mice were lethally irradiated by exposure to 10 Grey and reconstitute by intravenous injection of 100 μ l PBS containing one million BM cells from WT or *Gpr183* KO mice. Mice were analyzed 2-3 month after reconstitution.

2.2.10 NicheNet analysis: potential interactions between ligands from adventitial fibroblasts and target genes from *Mgl2*⁺ cDC2 cells

To predict which ligand-receptor interactions could potentially induce the DE genes found in cDC2 cells, we performed the NicheNet algorithm on a recently published scRNA murine lung dataset^[78, 79]. The Seurat package (V3.1.5) was applied to identify *Gpr183*⁺ cDC2 and adventitial fibroblasts from the scRNA dataset (GSE132771) and to determine DE genes in cDC2 cells.

Cells from untreated lung samples were loaded into the Seurat package. To produce the same number of clusters as shown in the published data, we used the first 20 dimensions and set the resolution as 0.6 to generate the UMAP. Next, the cluster with cells highly expressing *Cd86* and *Itgae* was annotated as the DC cluster. Within the DC cluster, we selected cells highly expressing *Mgl2* and *Gpr183* as our potential receiver cells (*Mgl2*⁺ cDC2). Simultaneously, the Seurat::FindMarker command was applied to identify DE genes for the receiver cells.

To identify adventitial fibroblasts, we subset GFP⁺ cells highly expressing *Col1* (Col-GFP⁺) from the previous Seurat object as described in the paper. Subsequently, the clustering analysis was performed on the Col-GFP⁺ adventitial fibroblasts. The adventitial fibroblasts from the cluster with DE genes of *Npnt*, *Pi16*, *Adh7*, *Dcn*, *Hhip*, and *Aspn* were defined as sender cells for downstream analysis.

Next, the NicheNet package (V0.1.0) was applied to predict which ligands produced by adventitial cells regulate target DE genes in the *Mgl2*⁺ cDC2 cells, according to the user manual.

2.2.11 Statistics

Statistical significance was determined using the two-tailed unpaired Student's T-test with at least 95% confidence. One-way analysis of variance was initially performed to determine whether an overall statistically significant change existed before using unpaired T-test. All statistical analyses were performed using the GraphPad Prism V8. Data were shown as mean \pm SD. * $P < 0.05$, ** $P < 0.01$, *** $P < 0.001$, and **** $P < 0.0001$ were all considered significant.

3 Results

3.1 Flow cytometric characterization of pulmonary mononuclear phagocytes

The lung hosts various myeloid cell populations, such as DCs, monocytes, macrophages and eosinophils, which play a crucial role in lung immunity. To discriminate each population accurately during homeostasis, we designed a multi-parameter panel and performed a sequential gating strategy (**Fig. 3-1A**). After the exclusion of doublets and debris by using FSC and SSC (forward scatter and side scatter, respectively), total myeloid cells were gated as CD45⁺Lin⁻ (Lin: CD3, CD19, B220, Ter119, Ly6G, and NK1.1). Dead cells were removed using live/dead staining. In the lung, both alveolar macrophages and eosinophils express SiglecF. Within SiglecF positive cells, the expression of CD64 and CD11c was used to distinguish alveolar macrophages (CD45⁺Lin⁻SiglecF⁺CD64⁺CD11c⁺) from eosinophils (CD45⁺Lin⁻SiglecF⁺CD64⁻CD11c⁻), allowing their unambiguous and clear identification. After excluding alveolar macrophages and eosinophils by gating the SiglecF negative fraction, total cDCs were identified based on their high expression of MHC2 and CD11c (MHC2⁺CD11c⁺), and their low expression of CD64 (macrophage marker) and Ly6C (monocyte marker). CD24 and CD11b were used to identify cDC1s (CD45⁺Lin⁻SiglecF⁻MHC2⁺CD11c⁺CD64⁻Ly6C⁻CD24⁺CD11b⁻) and cDC2s (CD45⁺Lin⁻SiglecF⁻MHC2⁺CD11c⁺CD64⁻Ly6C⁻CD24⁺CD11b⁺). As one of the heterogeneous cDC2s populations, CD301b⁺cDC2s constituting the majority of lung resident cDC2s (**Fig. 3-1A**) have been studied in multiple tissues, such as skin, LN, and lung. After the

exclusion of alveolar macrophages, eosinophils and cDCs, monocytes were characterized by the expression of CD11b and the absence of MHC2 (CD11b⁺MHC2⁻).

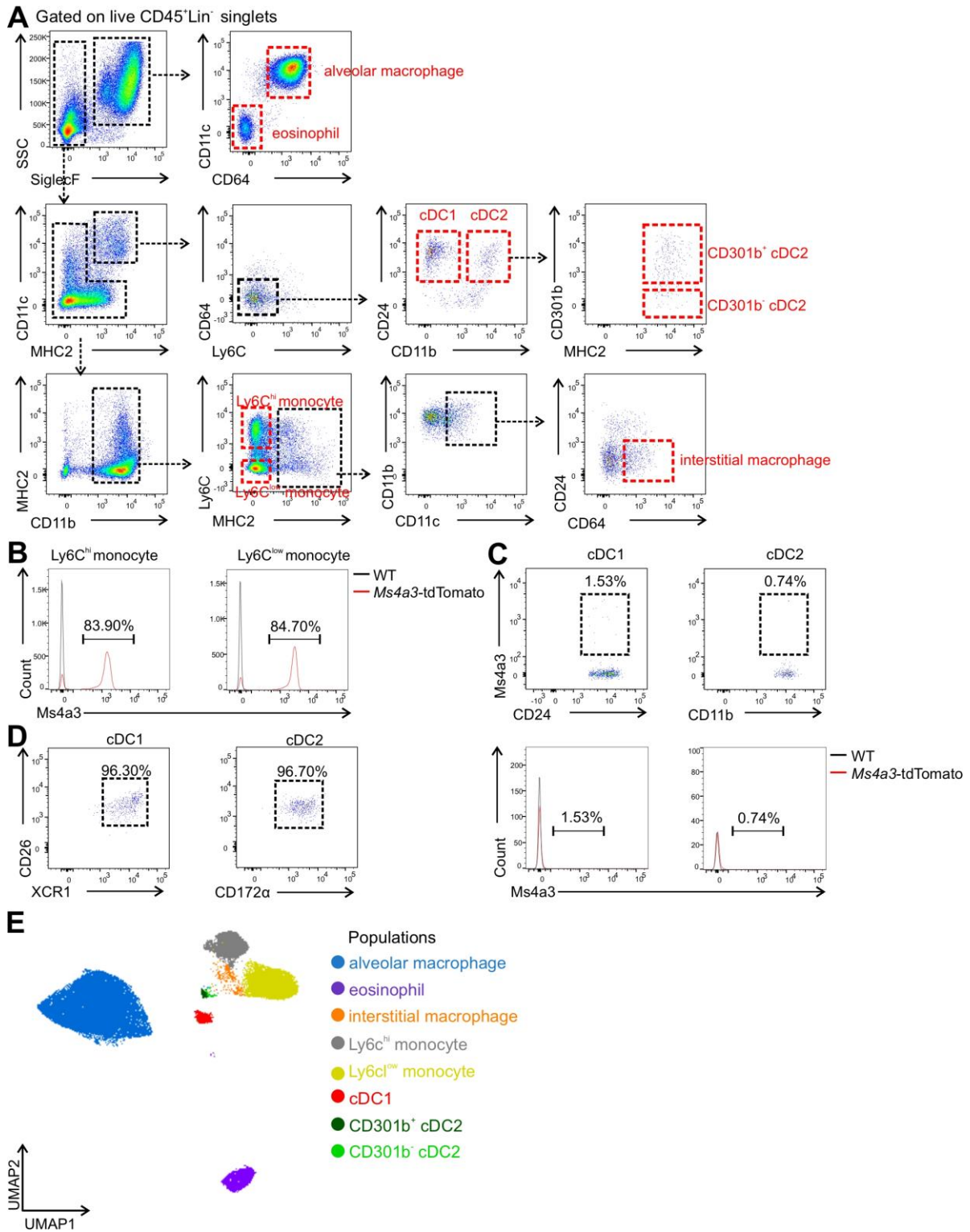


Figure 3-1. Identification of myeloid cell subsets with flow cytometry in murine lung. Cells isolated from enzymatically digested mouse lungs were stained and analyzed with flow cytometry. After excluding doublets and dead cells, total myeloid cells were gated as CD45⁺Lin⁻. (Lin: CD3, CD19, Ter119, NK1.1, B220, Ly6G) **(A)** Gating strategy to discriminate various subsets of myeloid cells, including alveolar macrophage (AM), interstitial macrophage, eosinophil, Ly6C^{hi} monocyte, Ly6C^{low} monocyte, cDC1, cDC2, CD301b⁺ cDC2 and CD301b⁻ cDC2. **(B, C)** *Ms4a3* labeling on monocyte (B) and cDC subsets (C) using *Ms4a3*^{cre}Rosa^{TdT} mice. **(D)** Validation of the identification of cDC1 and cDC2 with additional markers (CD26, XCR1 and CD172α). **(E)** Phenograph of myeloid cell clusters generated from uniform manifold approximation and projection (UMAP) analysis in WT mouse.

As an important branch of mononuclear systems in the lung, two subsets of monocytes can be found within the lung parenchyma and separated based on the expression of Ly6C; Classical monocytes or Ly6C^{hi} monocytes (CD45⁺Lin⁻SiglecF⁻MHC2⁻CD11b⁺Ly6C^{hi}), and Ly6C^{low} monocytes (CD45⁺Lin⁻SiglecF⁻MHC2⁻CD11b⁺Ly6C^{low}). Alveolar macrophages located in the airways are the main macrophage population in the murine lung. Non-alveolar macrophages, termed interstitial macrophages, also populate the murine lung. They are identified as CD45⁺Lin⁻SiglecF⁻MHC2⁺CD11b⁺CD11c⁺CD24⁻CD64⁺, and are localized in the interstitial part of the lung. Identification of a bona fide cDC compartment in the lung can be challenging^[26, 80]. To exclude possible monocytic contamination we utilized the *Ms4a3* fate mapping model, which allows for tracing of the monocyte lineage^[81] (**Fig. 3-1B, C**). As expected, monocytes were labeled with high levels of tdTomato (*Ms4a3*). None of the cDC1 and cDC2 populations were labeled with tdTomato (*Ms4a3*), as shown in the FACS plots

and histogram of **Fig. 3-1** (panels B and C), indicating their clean identity. Additional markers, such as CD26, XCR1, and CD172 α have been suggested to aid in the identification of bona fide cDC subsets in multiple tissues^[10]. Detection of these markers was useful to further validate the above-mentioned gating strategy (**Fig. 3-1A**). cDC1s (**Fig. 3-1A**) were found to be CD26⁺XCR1⁺ (**Fig. 3-1D**), while cDC2s (**Fig. 3-1A**) were CD26⁺CD172 α ⁺ (**Fig. 3-1D**). The myeloid compartment of the healthy murine lung was analyzed using this panel and cell populations were subjected to uniform manifold approximation and projection (UMAP). UMAP can project cell clusters at different distances to each other and the distances represent the biological differences between each cluster^[82]. As shown in **Fig. 3-1E**, 8 clusters of myeloid cells, including mononuclear phagocytes, were identified based on the expression of the selected markers, including CD45, SiglecF, CD64, CD11c, MHC2, Ly6C, CD11b, and CD24. Alveolar macrophages cluster farther away from eosinophils and DCs, whereas CD301b⁺ cDC2s and CD301b⁻ cDC2s were closer together (**Fig. 3-1E**) indicating biological similarity between cDC2s.

With a minimal set of core surface markers, it allows for the accurate and unambiguous identification of maximal subsets of myeloid cells in the murine lung under steady state, including alveolar macrophages, interstitial macrophages, eosinophils, subsets of monocytes, and subsets of cDCs, which paved the way to investigate the influence of GPR183 on various myeloid subsets.

3.2 *Gpr183* is abundantly expressed in cDCs, not in stromal cells

GPR183 was shown to be expressed in immune cells such as B cells, T-cells, and DCs in the spleen^[52, 59, 73]. Its expression and role in lung immune cells, especially in cDCs,

which play a critical role in the lung homeostasis, remain largely unknown. Before checking the role of GPR183 in pulmonary cDCs, its expression in the myeloid and stromal compartments of the lung was assessed by flow cytometry and qRT-PCR. For this purpose, we isolated cells from the lung in the *Gpr183*-flox-EGFP mouse line.

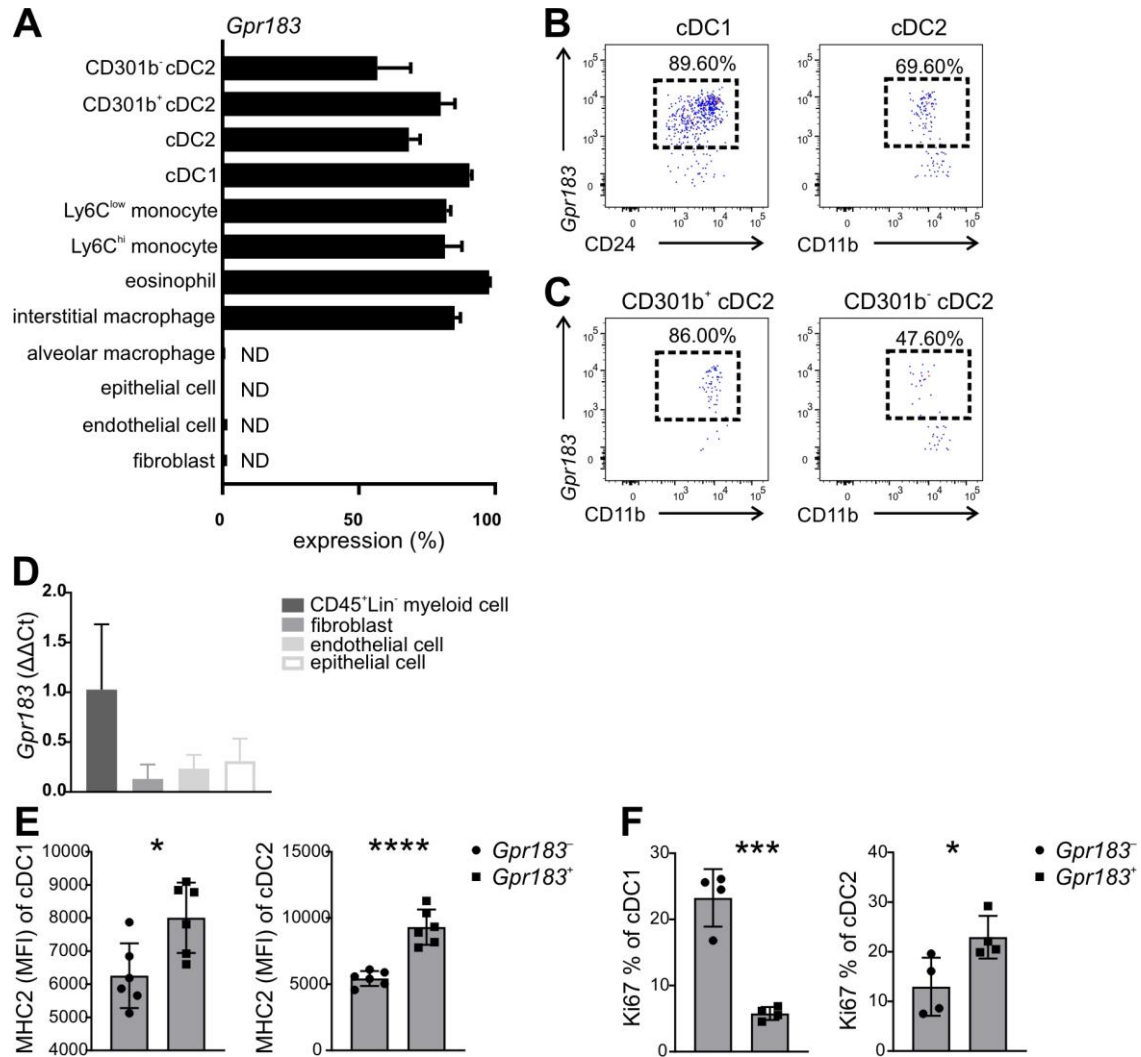


Figure 3-2. *Gpr183* is preferentially expressed on pulmonary myeloid cell subsets, not on stromal cell subsets. Stromal cell subsets and myeloid cell subsets isolated from enzymatically digested mouse lungs were stained and analyzed with flow cytometry. **(A)** *Gpr183* expression (indicated by EGFP expression) on stromal cell subsets (fibroblast, endothelial cell, and epithelial cell) and myeloid cell subsets in the lung of *Gpr183*-flox-EGFP mice (n = 3 or 4,

error bars represent mean \pm SD). **(B, C)** Representative FACS plots showing *Gpr183* expression on pulmonary (B) cDC1, cDC2, (C) CD301b⁺ cDC2 and CD301b⁻ cDC2 in *Gpr183*-flox-EGFP mice. Stromal cell subsets and total myeloid cells isolated from enzymatically digested mouse lungs were sorted. **(D)** Quantitative PCR analysis of *Gpr183* transcript abundance in sorted stromal and total CD45⁺Lin⁻ myeloid cell subsets from lungs of WT mice (n = 4, error bars represent mean \pm SD). Plot shows relative quantification normalized to the expression of the housekeeping gene *PPIA*. **(E, F)** Quantification of MHC2 (E) and Ki67 (F) expression on *Gpr183*⁻ and *Gpr183*⁺ fractions of pulmonary cDC1 or cDC2 cell subsets (n = 4 or 6, each dot represents a mouse, error bars represent mean \pm SD). **P* < 0.05, ****P* < 0.001, *****P* < 0.0001.

FACS analysis of cells from *Gpr183*-flox-EGFP mice in which EGFP reports the expression of *Gpr183* revealed that all myeloid cells, except for alveolar macrophages, express various levels of *Gpr183*, with the highest expression found on eosinophils (**Fig. 3-2A**). In contrast, all stromal cells, including epithelial cells, endothelial cells, and fibroblasts showed no expression of *Gpr183* (**Fig. 3-2A**). *Gpr183* was detected on both, cDC1s and cDC2s (**Fig. 3-2A, B**), which is consistent with previous the finding that GPR183 is expressed on splenic cDC1s and cDC2s^[52]. Analysis of cDC2 subsets revealed that a higher proportion of CD301b⁺ cDC2s (75%) was *Gpr183*⁺ compared with CD301b⁻ cDC2s (25%) (**Fig. 3-2A, C**). To confirm transcriptomic levels of *Gpr183*, total myeloid cells (CD45⁺Lin⁻) and three stromal cell populations were sorted from the WT lung and RNA was extracted from each population. In agreement with the flow cytometric analysis in the *Gpr183*-flox-EGFP mice, RNA transcripts of *Gpr183* were barely detectable in all three stromal cell populations, while there was a higher amount

of *Gpr183* in total myeloid cells (CD45⁺Lin⁻) (**Fig. 3-2D**). Taken together these results reveal that *Gpr183* shows a selective expression on myeloid cells, not on stromal cells in the murine lung.

3.3 *Gpr183*⁺ cDC2s show higher expression of maturation and proliferation in the murine lung

Proliferation and activation of cDCs are important for their maintenance and host defense in the lung. To investigate if there is a correlation between GPR183 expression and activation of DCs, MHC2 levels of pulmonary cDC1 and cDC2 were measured by flow cytometry. Higher levels of MHC2 were detected in *Gpr183*-expressing cDC1s and cDC2s than in *Gpr183*⁻ cDCs (**Fig. 3-2E**). Furthermore, *Gpr183*⁺ cDC1s showed lower proliferation than *Gpr183*⁻ cDC1s, while *Gpr183*⁺ cDC2s showed higher proliferation than *Gpr183*⁻ cDC2s (**Fig. 3-2F**), indicating that *Gpr183* regulates cDCs in a subset specific manner.

3.4 Genetic deletion of *Gpr183* leads to a deficiency in pulmonary cDC2 during homeostasis

It was shown that GPR183 guides the localization of cDC2s in the spleen and regulates their homeostasis and immunological function^[52, 71]. To provide insight into the role of GPR183 in pulmonary DCs, we assessed overall lung morphology and pulmonary myeloid cell abundance using flow cytometry (**Fig. 3-1A**) in WT and *Gpr183* deficient mice. Investigation of the overall lung morphology as assessed by H&E and alcian blue staining revealed no differences between WT and GPR183 deficient mice (**Fig. 3-3A**). Next lungs from WT and GPR183 deficient mice were assessed for changes on the cellular level using flow cytometry. This analysis revealed that GPR183 deficient mice

had decreased cDC2s, both in percentage and cell concentration (Fig. 3-3B, C, and D) whereas cDC1s only showed an increased percentage, but no effect on the cell concentration could be detected (Fig. 3-3B, C, and D).

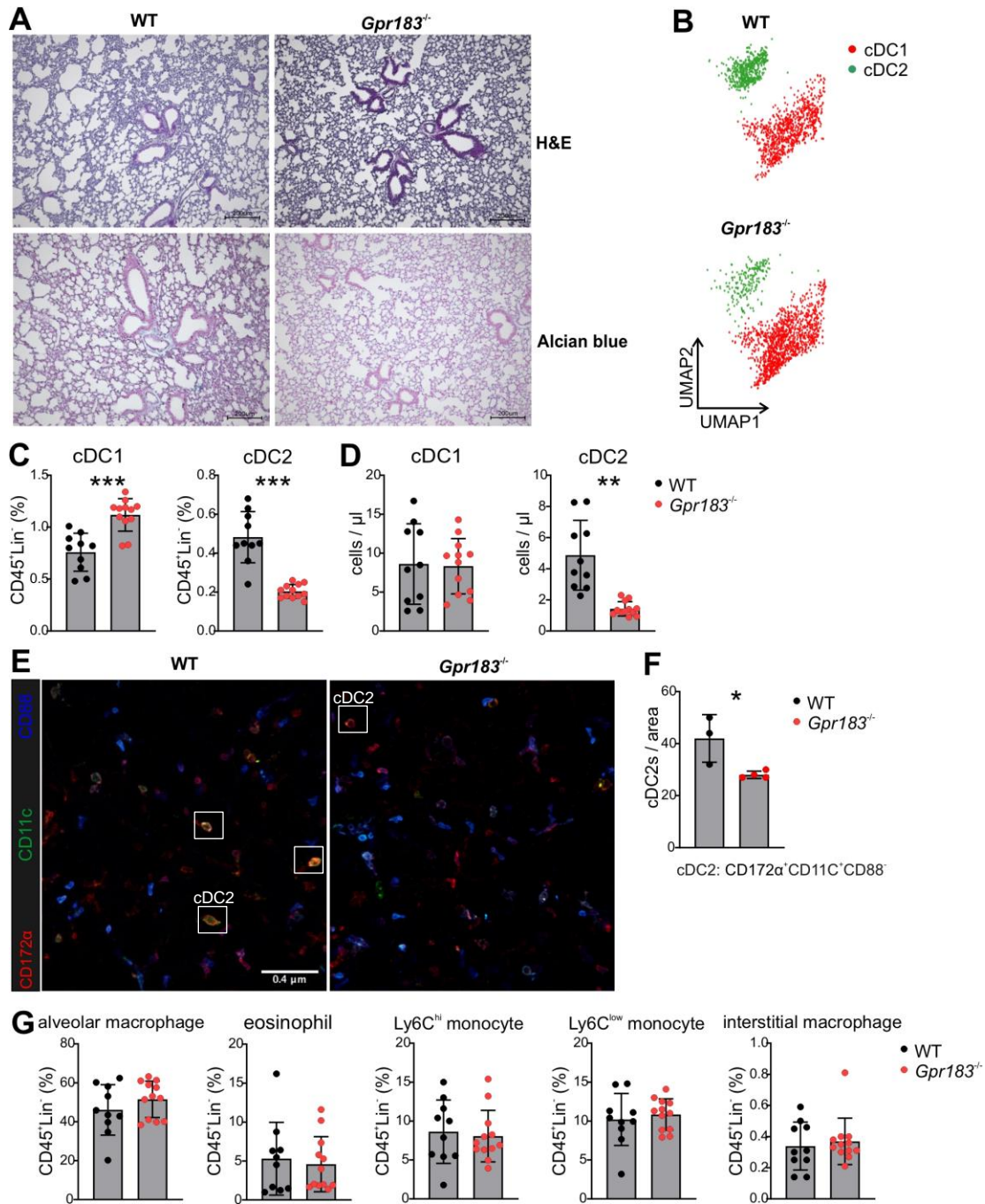


Figure 3-3. Ablation of GPR183 specifically decreases cDC2 population within myeloid cell subsets. (A) Hematoxylin and eosin (H&E; upper panel) and alcian blue (lower panel)

staining on paraffin embedded lung tissue (scale bars represent 200 μ m). **(B)** UMAP analyses and visualization of pulmonary CD45⁺Lin⁻CD64⁻Ly6C⁻MHC2⁺CD11c⁺CD24⁺ cells from WT and *Gpr183*^{-/-} mice. **(C, D)** Frequency (C) and cell concentration (D) of cDC1 and cDC2 cell subsets in the lung of WT (black dots) and *Gpr183*^{-/-} (red dots) mice (n = 10 or 12, each dot represents a mouse, error bars represent mean \pm SD). **(E)** Representative confocal images of PCLS of WT and *Gpr183*^{-/-} mice. Slices were immunostained using anti-CD11c (green), anti-CD172 α (red), and anti-CD88 (blue) antibodies to visualize cDC2 populations. Scale bars represent 0.4 μ m. **(F)** Quantification of cDC2s cell numbers per area (531 μ m X 531 μ m) in lung slices from (E) WT (black dots) and *Gpr183*^{-/-} (red dots) mice (n = 3, each dot represents a mouse, error bars represent mean \pm SD). **(G)** FACS analysis of the frequency of AMs, eosinophils, monocytes and interstitial macrophages in the lungs of WT (black dots) and *Gpr183*^{-/-} (red dots) mice (n = 10 or 12, each dot represents a mouse, error bars represent mean \pm SD). **P* < 0.05, ***P* < 0.01, ****P* < 0.001.

In order to visualize the reduction of cDC2 in the lung of GPR183 deficient mice *in situ*, live precision cut lung slice (PCLS) was generated and immunostained with a combination of antibodies against CD11c, CD172 α , and CD88, and sections were visualized with a confocal microscope^[51]. The abundance of pulmonary cDC2s (CD11c⁺CD172 α ⁺CD88⁺) was clearly reduced in *Gpr183*^{-/-} tissues (**Fig. 3-3E, F**) confirming the phenotype observed in flow cytometry (**Fig. 3-3C, D**).

Further we analyzed the effect of GPR183 deficiency on other cells of the myeloid compartment. As expected, AMs in the absence of GPR183 were unaffected (**Fig. 3-2A and 3-3G**). Interestingly, despite the high expression levels of *Gpr183* (**Fig. 3-2A**), the proportions of interstitial macrophages, eosinophils, and subsets of monocytes in

Gpr183^{-/-} mice remained unaltered (**Fig. 3-3G**). Taken together these results indicate a specific regulatory role of GPR183 in pulmonary cDC2.

3.5 GPR183 deletion results in a diminished migratory cDC2 compartment in the mediastinal lymph node

One of the main features of DC is its ability to migrate to draining LN in a CCR7-dependent manner and prime T cells differentiation^[1, 2, 83]. Since our results showed that the GPR183 deficiency leads to a diminished percentage and cell concentration of cDC2s in the lung, we next investigated whether migratory cDC1s and cDC2s in lung draining LN were also reduced. Migratory cDC2 (M-cDC2) showed decreased percentage and number within LN, while M-cDC1 remained unaffected (**Fig. 3-4A and 3-4B**) which indicated that GPR183 deficiency affected M-cDC2 in the lung draining LN.

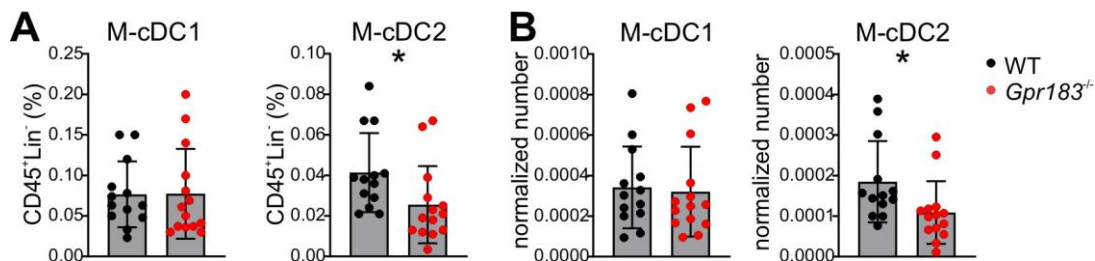


Figure 3-4. Ablation of GPR183 decreases migratory cDC2 population in the lung draining LN. Cells isolated from enzymatically digested mouse lung draining LN were stained and analyzed with flow cytometry. Frequency (**A**) and normalized numbers (**B**) of migratory cDC1s (M-cDC1s) and migratory cDC2s (M-cDC2s) in the LN of WT (black dots) and *Gpr183*^{-/-} (red dots) mice (n = 13 or 14, each dot represents a mouse, error bars represent mean ± SD). Normalized numbers = numbers of cDC1 or cDC2 / numbers of CD45⁺Lin⁻. **P* < 0.05.

3.6 Intrinsic expression of GPR183 is crucial for pulmonary cDC2 maintenance

We next examined whether the requirement of GPR183 for the maintenance of cDC2s in the lung was intrinsic. cDC composition was analyzed in mice with cDC specific ablation of GPR183, which were generated by crossing *Gpr183^{fl/fl}* mice with *Zbtb46-cre* mice, resulting in a specific deletion of GPR183 in DCs. ZBTB46 was identified as a TF selectively expressed by cDC and its committed progenitors. pDCs, monocytes, or other cell types of the lymphoid or myeloid lineages do not express it^[11]. The progeny from *Gpr183^{fl/fl}Zbtb46-cre⁺* mice showed decreased frequency and cell concentration of total cDC2s as compared to the *Zbtb46-cre⁺* littermate control mice (**Fig. 3-5A, B, and C**), which is consistent with the phenotype observed in *Gpr183^{-/-}* mice. As expected, cDC1s remained unaffected in *Gpr183^{fl/fl}Zbtb46-cre⁺* mice. It is known that cDC2s comprise rather heterogeneous populations which appear to have different functions. CD301b⁺ cDC2s, were reported largely to be present in the skin and draining LN and demonstrated the ability to efficiently prime Th2 and Th17 T-cell responses, which was also observed recently in the lung^[33, 36]. Hence, we investigated whether CD301b⁺ or CD301b⁻ cDC2 were primarily affected by DC specific genetic deletion of GPR183. Both CD301b⁻ cDC2s and CD301b⁺ cDC2s were affected by GPR183 ablation and showed lower numbers in *Gpr183^{fl/fl}Zbtb46-cre⁺* mice compared to littermate control mice (**Fig. 3-5D and E**).

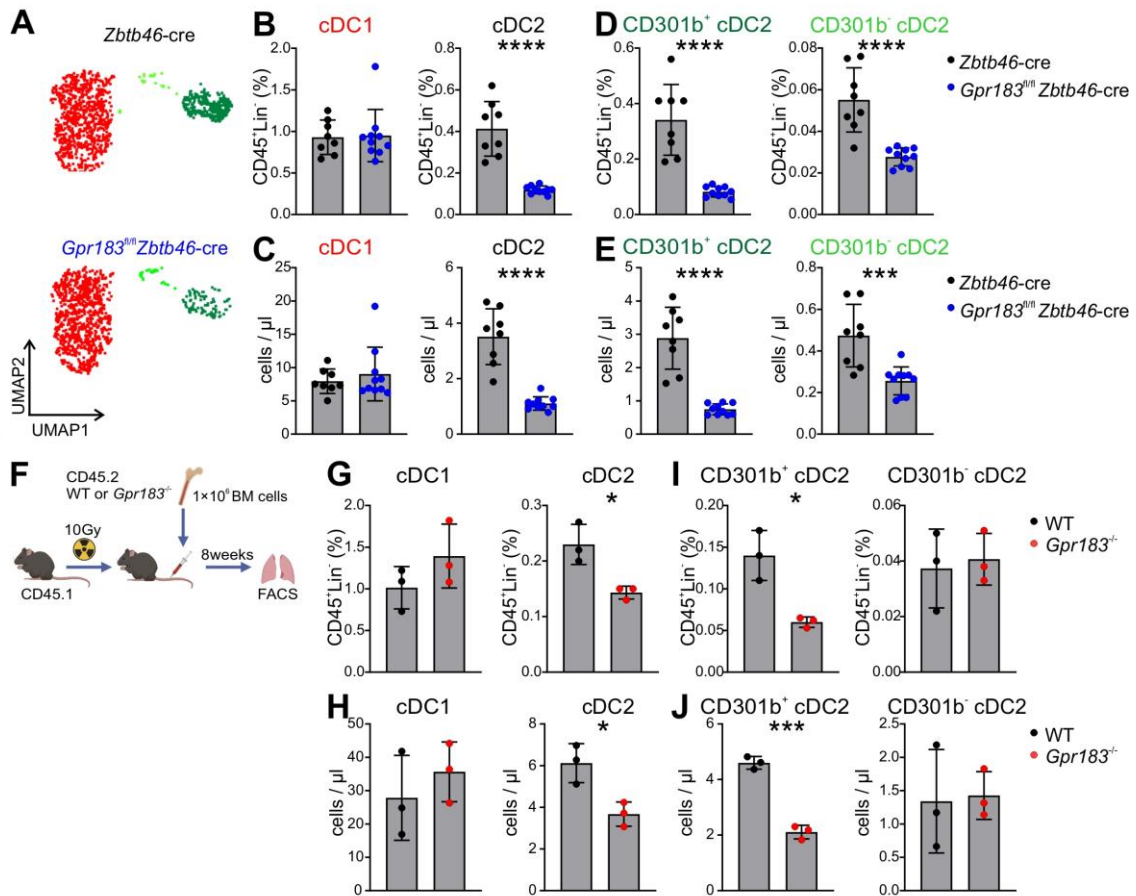


Figure 3-5. Maintenance of pulmonary cDC2 depends on intrinsic expression of GPR183.

Cells isolated from enzymatically digested mouse lungs were stained and analyzed with flow cytometry. **(A)** UMAP analysis and visualization of pulmonary CD45⁺Lin⁻CD64⁻Ly6C⁻MHC2⁺CD11C⁺CD24⁺ cells in *Gpr183^{fl/fl};Zbtb46-cre* mice (lower panel) and littermate controls (*Zbtb46-cre*; upper panel). **(B, C)** FACS analysis of cDC1 and cDC2 subpopulations in lungs of *Gpr183^{fl/fl};Zbtb46-cre* (blue dots) and *Zbtb46-cre* (black dots) mice. Plots show the frequency (B) and concentration (C) of cDC1s and cDC2s (n = 8 or 10, each dot represents a mouse, error bars represent mean ± SD). **(D, E)** FACS analysis of CD301b⁺ cDC2s and CD301b⁻ cDC2s subsets in lungs of *Gpr183^{fl/fl};Zbtb46-cre* (blue dots) and *Zbtb46-cre* (black dots) mice. Plots show the frequency (D) and concentration (E) of cells (n = 8 or 10, each dot represents a mouse, error bars represent mean ± SD). **(F)** Schematic representation of the generation of

Gpr183^{-/-} and WT bone marrow chimeras. CD45.2 BM cells from WT or *Gpr183*^{-/-} mice were injected intravenously (i.v.) into CD45.1 recipient mice. 8 weeks later, pulmonary cDC1, cDC2 and cDC2 subsets from donors were analyzed with flow cytometry. **(G, H)** Frequency (G) and concentration (H) of pulmonary cDC1 and cDC2 in WT (black dots) and *Gpr183*^{-/-} (red dots) mice from donors' contribution (CD45.2) (n = 3, each dot represents a mouse, error bars represent mean ± SD). **(I, J)** Frequency (I) and concentration (J) of pulmonary CD301b⁺ cDC2s and CD301b⁻ cDC2s subsets in WT (black dots) and *Gpr183*^{-/-} (red dots) mice from donors' contribution (n = 3, each dot represents a mouse, error bars represent mean ± SD). **P* < 0.05, ****P* < 0.001, *****P* < 0.0001.

To further confirm that intrinsic GPR183 expression in cDC2 is needed to regulate the abundance of cDC2 in the lung, we generated BM chimeras by reconstituting lethally irradiated C57BL/6 congenic B6.SJL-Ptprc^a (CD45.1) mice with 1 million *Gpr183*^{-/-} (CD45.2) or littermate control (CD45.2) total BM cells **(Fig. 3-5F)**. 8 weeks after reconstitution, subsets of cDCs in the lung originating from *Gpr183*^{-/-} (CD45.2) or littermate control (CD45.2) were assessed with flow cytometry. cDC2s originating from *Gpr183*^{-/-} had a much lower percentage and cell concentration than did littermate controls **(Fig. 3-5G and H)**, indicating that GPR183 deficient cDC2s were impaired in reconstituting the cDC2 compartment after irradiation if they lack GPR183 expression. The same phenotype was observed for CD301b⁺ cDC2s, while the percentage and number of cDC1s were intact in the KO group **(Fig. 3-5I and J)**. These results suggested that DC specific GPR183 deficiency results in a selective decrease of cDC2s, leading to a specific reduction of the CD301b⁺ cDC2 subset due to the intrinsic role of GPR183 in cDC2.

3.7 DC specific ablation of GPR183 decreases pulmonary cDC2 proliferation

To determine whether the reduction of cDC2s in GPR183 deficient mice was caused by dysregulation of proliferation or apoptosis, we measured the expression of Ki67 (proliferation marker), annexin V (AnnV, apoptosis marker), and caspase 3 (apoptosis marker) within the pulmonary cDC compartment of *Gpr183*^{-/-} and WT mice. To exclude cDC-extrinsic factors that affect proliferation, *Gpr183*^{fl/fl}*Zbtb46-cre*⁺ and *Zbtb46-cre*⁺ mice were used. Ki67, widely used as a proliferation marker^[84, 85], showed decreased expression in cDC2s from *Gpr183*^{-/-} or *Gpr183*^{fl/fl}*Zbtb46-cre*⁺ mice compared to their littermate controls (**Fig. 3-6A, B and C**). As a control, the percentage of cDC1s expressing Ki67 was investigated and shown to be similar between *Gpr183*^{-/-} or *Gpr183*^{fl/fl}*Zbtb46-cre*⁺ and littermate controls (**Fig. 3-6A, B and C**).

To establish whether GPR183 had a role in the regulation of cDC apoptosis, we compared the frequency of cDCs undergoing apoptosis indicated by the expression of AnnV or caspase-3. AnnV was used together with fixable viability dye (FVD) to determine different stages of apoptosis. Double-positive (AnnV⁺FVD⁺) cells were in late-stage apoptosis, whereas AnnV single positive cells were undergoing early-stage apoptosis. Pulmonary cDC1s and cDC2s undergoing early and late stages of apoptosis remained unchanged between WT and KO groups (**Fig. 3-6D**). However, the flow cytometric assessment of active caspase-3 quantified in cDC populations showed a significant enhancement in cDC2 within the KO group (**Fig. 3-6E**). Together these data indicate that GPR183 regulates cDC2 maintenance in the lung by influencing their proliferative capacity and their survival.

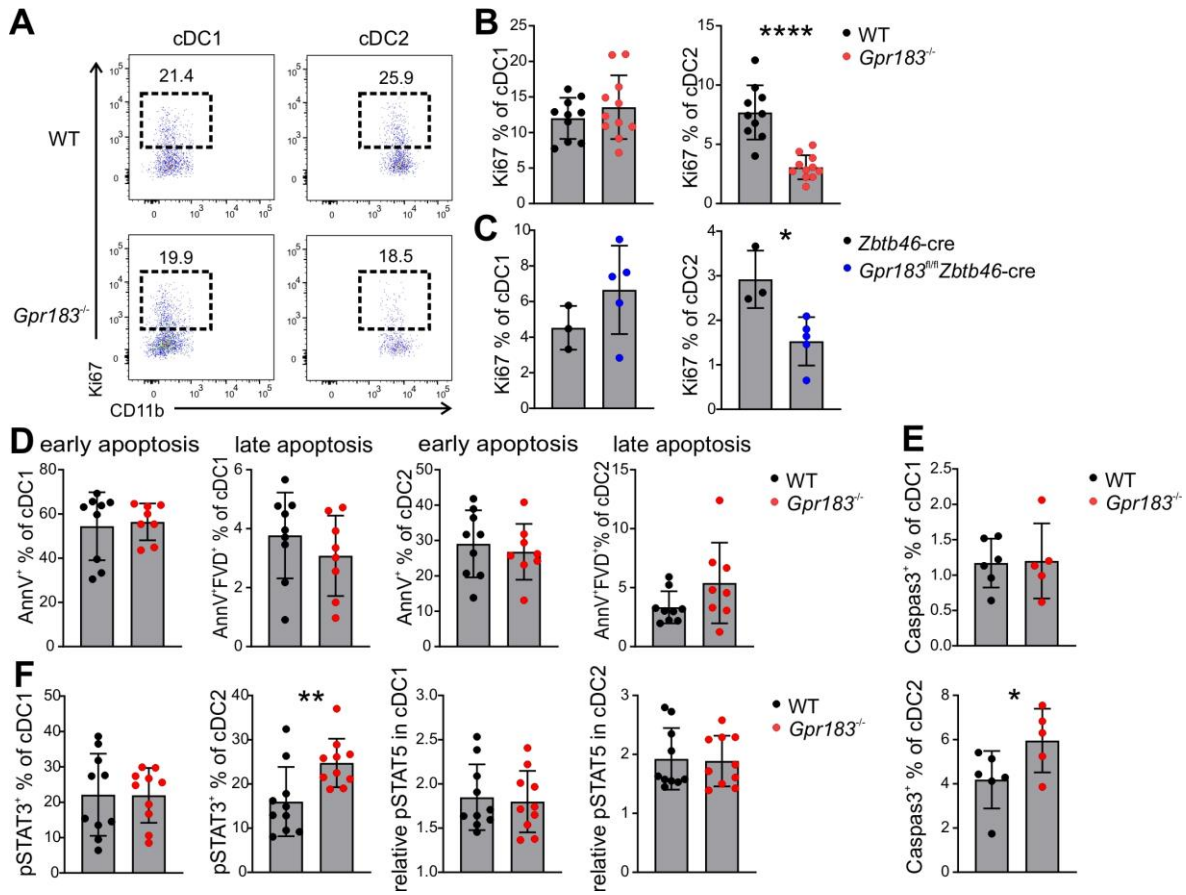


Figure 3-6. GPR183 deficiency impairs proliferation and apoptosis of cDC2. Cells isolated from enzymatically digested mouse lungs were intracellularly stained and analyzed with flow cytometry. **(A)** Representative FACS plots showing Ki67 expression on cDC1 and cDC2 in the lungs of WT (upper panels) and *Gpr183*^{-/-} (lower panels) mice. **(B)** Frequency of Ki67-positive cells on cDC1 and cDC2 subsets in lungs of WT (black dots) and *Gpr183*^{-/-} (red dots) mice (n = 10 or 11, error bars represent mean ± SD). **(C)** Frequency of Ki67-positive cells on cDC1 and cDC2 in the lungs of *Gpr183*^{fl/fl}*Zbtb46-cre* (blue dots) and *Zbtb46-cre* (black dots) mice (n = 3 or 5, each dot represents a mouse, error bars represent mean ± SD). **(D)** Percentage of annexin V⁺ (annV⁺) or annV⁺FVD⁺ cDC1 and cDC2 in the lungs of WT (black dots) and *Gpr183*^{-/-} (red dots) mice (n = 8 or 9, each dot represents a mouse, error bars represent mean ± SD). **(E)** Proportion of pulmonary cDC1 and cDC2 cells expressing active caspase 3 in the lungs of WT (black dots) and *Gpr183*^{-/-} (red dots) mice (n = 8 or 9, each dot represents a mouse, error bars

represent mean \pm SD). **(F)** Proportion of cDC1 and cDC2 cells that express phosphorylated STAT3 (pSTAT3) and phosphorylated STAT5 (pSTAT5) in the lungs of WT (black dots) and *Gpr183*^{-/-} (red dots) mice (n = 10, each dot represents a mouse, error bars represent mean \pm SD). **P* < 0.05, ***P* < 0.01, *****P* < 0.0001.

It was previously reported that STAT3 and STAT5 are involved in the regulation of cDC maintenance or function^[86-89]. Decreased phosphorylation of STAT3 in IL-6 KO mice resulted in an increased number of DCs^[87] indicating that STAT3 negatively regulates the DC number. To explore this in our experimental setting, the expression of phosphorylated STAT3 (pSTAT3) in pulmonary cDC2 from *Gpr183*^{-/-} or WT animals was assessed and showed an increased percentage of pSTAT3 (**Fig. 3-6F**) in line with previous mechanistic data and likely contributing to the loss of pulmonary cDC2 in the absence of GPR183.

3.8 GPR183 expression is not required for normal DC development

Development of DCs follows a gradual process, from early precursors to DC committed progenitors in BM. Pre-DCs leave the BM, seed peripheral tissues, and further differentiate into DC^[42]. We next determined whether GPR183 signaling directly regulates cDC2s or their committed progenitors. First, we investigated whether or not GPR183 is expressed in MDP, CDP, pre-cDC1, and pre-cDC2 in the BM, blood, and lung using *Gpr183*-flox-EGFP mice. The representative gating strategy for BM samples is shown in **Fig. 3-7A**. Both pre-cDC1 and pre-cDC2 expressed high levels of *Gpr183* in the BM, blood, and lung (**Fig. 3-7B**). MDP and CDP, early progenitors of DC, also expressed different levels of *Gpr183*, with 46.68% on MDP and 20.40% on CDP (**Fig. 3-**

7B). MDP and CDP from *Gpr183* deficient mice were unaffected, despite their expression of *Gpr183* (**Fig. 3-6C**). In addition, the percentage of pre-cDC, pre-cDC1, and pre-cDC2 remained the same between WT and *Gpr183*^{-/-} groups in BM, blood, and lung (**Fig. 3-7D**), suggesting that GPR183 is not required for the normal early development of DCs.

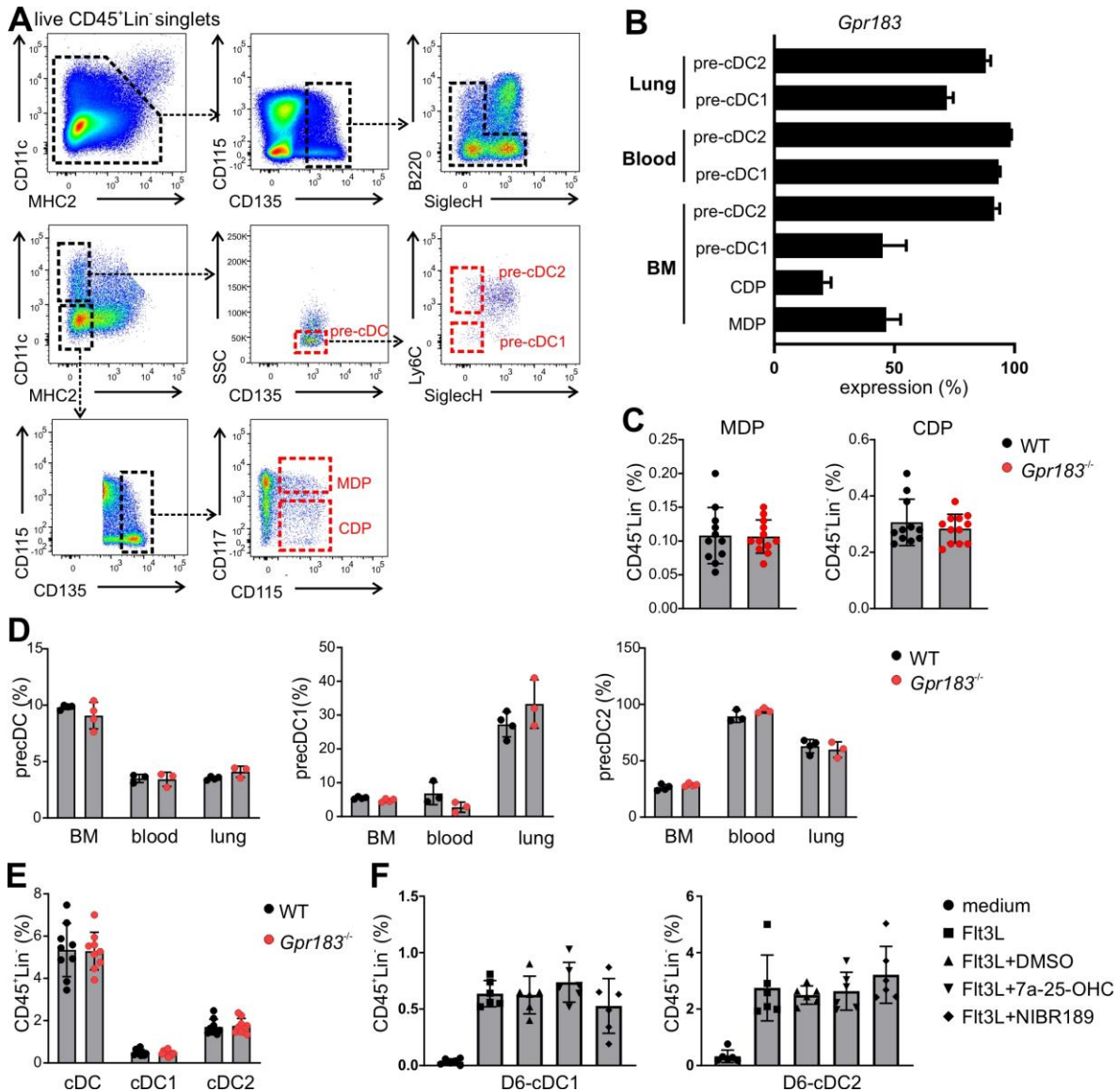


Figure 3-7. GPR183 is not required for the cDC development. BM cells flushed from tibia and femur were stained and analyzed with flow cytometry. **(A)** Gating strategy to discriminate

MDP, CDP, pre-cDC, pre-cDC1, and pre-cDC2 in the BM of WT mice. **(B)** Frequency of *Gpr183* expressing MDP, CDP, pre-cDC, pre-cDC1 and pre-cDC2 in BM, blood and lung of WT mice (n = 3 or 4, error bars represent mean \pm SD). **(C)** Frequency of MDP and CDP in the BM of WT (black dots) and *Gpr183*^{-/-} (red dots) mice (n = 11 or 12, error bars represent mean \pm SD). **(D)** Frequency of pre-cDC, pre-cDC1 and pre-cDC2 in the indicated organs in WT (black dots) and *Gpr183*^{-/-} (red dots) mice (n = 3 or 4, error bars represent mean \pm SD). BM cells isolated from WT or *Gpr183*^{-/-} mice were culture with FLT3L *in vitro*. At day 7, cultured BM cells were stained and analyzed with flow cytometry. **(E)** Frequency of total cDC and cDC subsets generated *in vitro* from WT and *Gpr183*^{-/-} BM cultured with FLT3L (n = 9, Error bars represent mean \pm SD). **(F)** Frequency of cDC1 and cDC2 generated *in vitro* from WT BM cultured with FLT3L, supplement with or without DMSO, 7 α ,25-OHC and NIBR189 (n = 6, error bars represent mean \pm SD).

To further explore the role of GPR183 in the cDC development *in vitro*, BM from WT or *Gpr183*^{-/-} mice was cultured in the presence of FLT3L, as cDC development depends on the growth factor FLT3L and its receptor FLT3 (CD135)^[46], expressed on cDC precursors. On day 6, cultured BM cells were analyzed by flow cytometry and cDC subsets frequencies and numbers were investigated. This analysis showed that GPR183 deficient BM derived cDC subsets were as abundant as their WT counterparts within the FLT3L *in vitro* cultures **(Fig. 3-7E)**. Next, we evaluated the effect of pharmacological activation or inhibition of GPR183 on cDC development *in vitro*. To this end we added in addition to FLT3L either the GPR183 agonist (7 α ,25-OHC) or the antagonist (NIBR189) into the culture medium and analyzed the frequency and abundance of cDC1 and cDC2 after 6 days of culture. Here no effect of either activation

or inhibition of GPR183 signaling could be observed with similar numbers of cDC1 and cDC2 present after 6 days of culture with either the agonist (7 α ,25-OHC) or the antagonist (NIBR189) further confirming that DC development is not dependent on the GPR183 *in vitro*.

3.9 Genetic deletion of *Ch25h* leads to a deficiency of pulmonary cDC2 during homeostasis

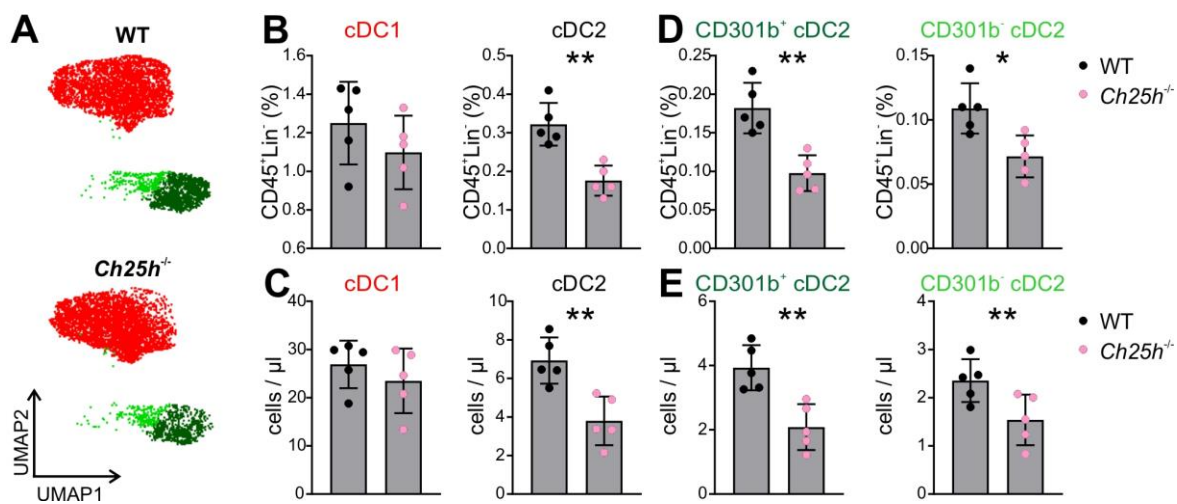


Figure 3-8. Loss of CH25H diminishes pulmonary cDC2. (A) UMAP analysis and visualization of pulmonary CD45⁺Lin⁻CD64⁻Ly6C⁻MHC2⁺CD11C⁺ cells in WT and *Ch25h*^{-/-} mice. (B, C) Frequency (B) and cell concentration (C) of cDC1 and cDC2 in the lung of WT (black dots) and *Ch25h*^{-/-} (pink dots) mice (n = 5, Error bars represent mean \pm SD). (D, E) Frequency (D) and cell concentration (E) of CD301b⁺ cDC2s and CD301b⁻ cDC2s in the lungs of WT (black dots) and *Ch25h*^{-/-} (pink dots) mice (n = 5, each dot represents a mouse, error bars represent mean \pm SD). *P < 0.05, **P < 0.01.

Mice deficient in the biosynthetic enzyme CH25H are impaired in synthesizing 7 α ,25-OHC, the natural and selective ligand of GPR183. A prior report indicated that CH25H

deficient mice show decreased cDC2 numbers and altered cDC2 localization in the spleen^[71]. To investigate whether production of 7 α ,25-OHC by CH25H is crucial for cDC2 homeostasis in the lung we investigated the cDC2 compartment in CH25H deficient mice in vivo. Mice deficient in CH25H showed similar cDC1 concentrations and percentage between WT and *Ch25h* knockout mice, whereas both cDC2 concentration and abundance was significantly lower compared to WT mice (**Fig. 3-8A, B, and C**). Next, we wanted to assess whether both CD301b⁺ and CD301b⁻ cDC2 were affected by the loss of CH25H. These results showed that both CD301b⁺ cDC2s and CD301⁻ cDC2s were affected equally (**Fig. 3-8D and E**). Taken together these data demonstrate that 7 α ,25-OHC is essential for the maintenance of cDC2s and cDC2s' subsets and that CH25H catalyzed biosynthesis of 7 α ,25-OHC affect the cDC2 compartment in the lung similar to the loss of GPR183. Overall, the total cDC2s were less affected in *Ch25h*^{-/-} than in *Gpr183*^{-/-} mice.

3.10 Fibroblasts produce key enzymes related to GPR183 ligand and regulate cDC2s via TSLP-CRLF2 (TSLPR)

Cell type specific expression of the rate limiting enzymes involved in the biosynthesis of 7 α ,25-OHC is largely unknown. To better understand the cell type specific expression of the key rate limiting enzymes involved in the biosynthesis of 7 α ,25-OHC, *Ch25h*, *Cyp7b1* and *Hsd3b1* we performed a real time PCR analysis of the mRNA levels of these key enzymes in flow cytometrically purified total myeloid cells, fibroblasts, endothelial and epithelial cells of WT lung. Total myeloid cells and endothelial cells expressed *Ch25h* and *Hsd3b1*, while epithelial cells showed undetectable expression of any of the three enzymes (**Fig. 3-9A**). Fibroblasts were the only population that besides

expressing *Ch25h* also expressed *Cyp7b1*, both of which are crucial rate limiting enzymes within the production cascade of the GPR183 ligand $7\alpha,25\text{-OHC}$ ^[71].

The expression pattern of the three enzymes observed in the qRT-PCR experiments indicated that lung fibroblasts had the potential to regulate cDC2s since it was the only population among the stromal and myeloid compartments expressing both, *Ch25h* and *Cyp7b1*. To prove this, we performed imaging experiments in living tissue and investigated the spatial interaction of cDC2s ($\text{CD11c}^+\text{CD172a}^+\text{CD88}^-$) with fibroblasts ($\text{PDGFR}\alpha^+$) in the lung, in the presence and absence of GPR183 (**Fig. 3-9B**). We detected and quantified the number of cDC2s which were close and far to fibroblasts. This analysis showed that only the cDC2s closely associated with fibroblasts were affected by the ablation of GPR183 (**Fig. 3-9C**) suggesting that the maintenance of cDC2s was dependent on fibroblasts.

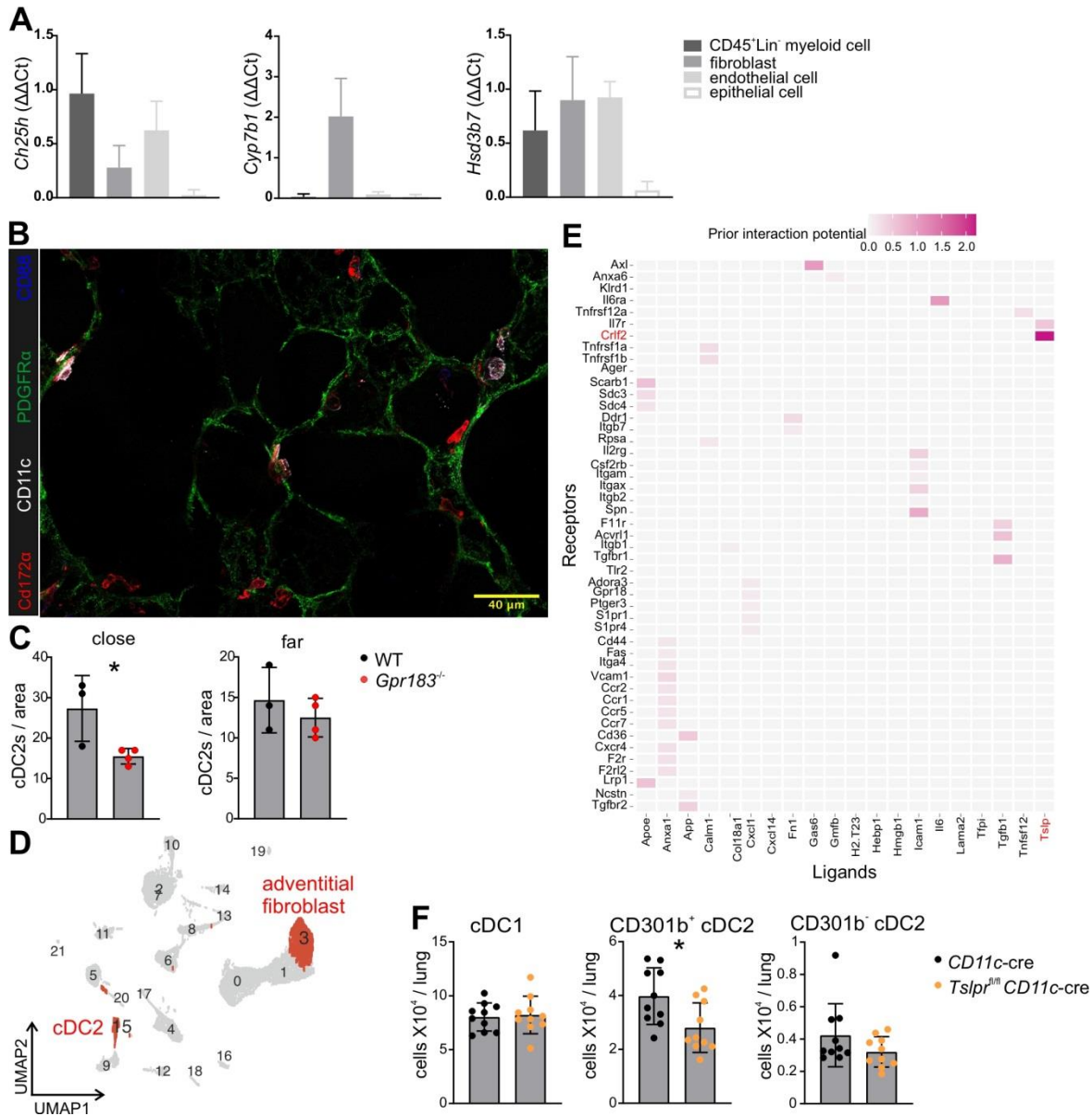


Figure 3-9. TSLP – CRLF2 (TSLP) axis is critical to maintain pulmonary cDC2. (A)

Quantitative PCR analysis of *Ch25h*, *Cyp7b1* and *Hsd3b7* transcript abundances in sorted stromal cell populations and CD45⁺Lin⁻ cells from WT mice lungs ($n = 4$, Error bars represent mean \pm SD). Plots show relative quantification normalized to the expression of the housekeeping gene *PPIA*. **(B)** Representative confocal images of precision cut lung slices of WT mice. Slices were immunostained using anti-CD11c (white), anti-CD172 α (red), anti-PDGFR α (green), and anti-CD88 (blue) antibodies to visualize cDC2s and fibroblasts. Scale bar

represents 40 μm . **(C)** Quantification of the number of cDC2 cells (from confocal images of (B)) which are in close and far proximity to fibroblasts in PCLS ($n = 3$, error bars represent mean \pm SD). **(D)** UMAP identification of CD301b⁺ cDC2 and adventitial fibroblast from the murine WT lung. **(E)** NicheNet analysis of potential interactions between receptors on cDC2 and ligand on fibroblast from the murine WT lung. **(F)** Absolute number of cDC1s, CD301b⁺ cDC2s and CD301b⁻ cDC2s in the lungs of *Tsfp^{fl/fl}CD11c-cre* (orange dots) and *CD11c-cre* (black dots) mice ($n = 9$ or 10 , Error bars represent mean \pm SD). * $P < 0.05$.

Tissue niche is emerging as a microenvironment which exists in different tissues imprinting identity, phenotype, or function of contacting cells. Modification of tissue niches can happen during inflammation which induces the identity or phenotype switch of contacting cells and facilitates the resolution of inflammation. For example, vascular endothelial cell niche in the murine lung is essential for interstitial macrophages reprogramming as Rspodin3 released by endothelial cells activates β -catenin signaling in interstitial macrophages which are located in close proximity to the lung vascular endothelial niche. Rspodin3- β -catenin axis induces metabolic and epigenetic reprogramming of interstitial macrophages^[90]. Cell-cell contact via ligand-receptor interaction is one of the ways by which tissue niches may regulate neighboring cells' function and / or maintenance. To predict the potential regulatory ligand-receptor interactions between cDC2s and fibroblasts, we took advantage of a recently published single cell transcriptomics dataset of cDC2s and fibroblasts isolated from a healthy murine lung^[79, 91] and performed NicheNet analysis. Adventitial fibroblasts were identified in cluster 3 and CD301b⁺ cDC2s were identified in cluster 15 (**Fig. 3-9D**). Thymic stromal lymphopoietin (*Tsfp*) from fibroblasts and cytokine receptor like factor 2

(*Crlf2*) from cDC2s was the pair that showed the highest interaction potential (**Fig. 3-9E**). TSLP is mostly produced by endothelial cells, fibroblasts, and exert its biological function through TSLPR (CRLF2). TSLP has been shown to stimulate DCs and further induce adaptive immune-mediated type 2 airway inflammation^[92, 93]. When ligation of TSLP with TSLPR was disrupted, pulmonary CD301b⁺ cDC2s were selectively decreased in the *Tslpr* KO mice (**Fig. 3-9F**). These results suggest that fibroblasts are the local producers of enzymes to generate GPR183 ligands and regulate maintenance of cDC2s potentially via TSLP-CRLF2 (TSLPR).

4 Discussion

In this study, we investigated the role of GPR183 in pulmonary cDC2s and its role in cDC2s : fibroblasts crosstalk within the murine lung. We showed that GPR183⁺ cDC2s sit closer to CH25H⁺CYP7B1⁺ fibroblasts, where GPR183⁺ cDC2s got niche-specific signals from neighboring fibroblasts, such as TSLP, contributing to the maintenance of cDC2s by regulating their proliferation and apoptosis. First, we found that GPR183 played an intrinsic role in the maintenance of pulmonary cDC2s. Second, development of cDCs was not controlled by GPR183 as cDCs develop normally *in vivo* and *in vitro* in the absence of GPR183. Third, we established that the GPR183 – 7 α ,25-OHC axis was critical for cDC2s' maintenance in the lung. Finally, NicheNet predicted that fibroblasts were critical to provide a niche to cDC2 by producing TSLP which was important for cDC2 maintenance in the lung.

The lung is constantly exposed to pathogens, allergens or pollutants. Among lung resident immune cells, cDCs actively survey the lung tissue during homeostasis and play a critical role in guarding the host due to their capacity to link innate and adaptive immunity. Therefore, maintaining a finely tuned lung resident cDC compartment is essential for host defense and proper lung function. A variety of transcriptional and epigenetic factors have been shown to facilitate the development or function of either cDC1s or cDC2s^[94, 95]. However, how cDCs strategically locate in a subset specific manner within the lung microenvironment remains elusive. As a chemotactic receptor, GPR183 is the first cell surface receptor shown to be required for intra-tissue positioning of splenic cDC2s^[52]. It was reported that the lung showed a high expression of

Gpr183^[53], which made it an ideal candidate receptor to regulate the localization of pulmonary cDCs.

4.1 Unambiguous discrimination of *bona fide* cDCs and the expression pattern of *Gpr183*

Discrimination of various myeloid cell subsets in the lung can be very challenging. To study the role of GPR183 on pulmonary cDCs in mice, a panel for flow cytometric analysis was designed, which unambiguously discriminates cDC subsets from other lung resident myeloid cell subsets, in particular macrophages and monocytes. *Bona fide* cDCs are positive for CD26, with the expression of XCR1 on cDC1s and CD172 α on cDC2s^[10]. To further corroborate the efficacy and accuracy of the panel, flow cytometric data were analyzed using UMAP and subsequent clustering analysis via Phenograph. Unsupervised clustering analysis showed that pulmonary cDC subsets clearly clustered without any overlap with each other, validating our panel. The clear and unambiguous discrimination of cDCs using flow cytometry and computational analysis was a relevant starting point for further study the role of GPR183 in the lung resident cDC development and function. We also validated this panel in other murine tissues, such as spleen, liver and skin, which were not shown in this thesis.

Gpr183 is widely expressed by many immune cells in various murine tissues, such as spleen, intestine, and LN^[52, 56, 73]. In the spleen and the LN, studies on *Gpr183* expression focused on cDCs, B cells, and T cells^[52, 65]. However, its expression pattern in the lung had not been investigated. In this work, we evaluated the expression levels of *Gpr183* in different lung resident subsets of the stromal and myeloid cells, including cDCs, and found that myeloid cells are the main expressers of *Gpr183* in the murine

lung, suggesting a possible role of *Gpr183* on myeloid cell function, development or homeostasis as it has been shown for splenic cDCs. Furthermore, similar to the spleen^[52], pulmonary cDC1s and cDC2s also express high level of *Gpr183*. Showing the expression pattern of *Gpr183* in various myeloid cell subsets, our data add the complexity of the cellular expression of *Gpr183*.

4.2 GPR183 regulates maintenance of cDC2s and their subsets intrinsically

Most of the extant data on the function of GPR183 has been obtained in the context of its function as a chemotactic receptor involved in the migration of B and T cells. Its role in the regulation of DCs remains poorly understood. We first performed H&E and alcian blue stainings to determine if GPR183 is important to maintain the morphology and structure of the lung, but no signs of inflammation or disrupted lung structure in WT or *Gpr183*^{-/-} mice were observed during homeostasis. Furthermore, other groups have reported that GPR183 was critical in the regulation of splenic cDC2s but not of cDC1s, even though the latter ones expressed *Gpr183*^[52, 57]. In line with this, we also observed a reduction of pulmonary cDC2s in the absence of *Gpr183* but not of cDC1. *Gpr183* showed a specific effect on cDC2s among all the *Gpr183* positive pulmonary mononuclear phagocytes. Several studies have shown the phenotypic and functional heterogeneity of the cDC2 compartment across several organs. For example, CD301b/MGL2 mainly expressed on cDC2, has been associated with Th2 and Th17 responses in the skin and LN respectively^[34, 96]. Additionally, murine CD301b⁺ cDC2s are akin to human T-bet⁻ cDC2s which have shown pro-inflammatory potential^[33]. As the majority of cDC2 subsets, pulmonary CD301b⁺ cDC2s also decreased in the absence of

Gpr183, suggesting a similar role of *Gpr183* may exist in human lung cDC2s, as human T-bet⁻ cDC2s are the equivalent of mouse CD301b⁺ cDC2s. Our work not only delineates the role of *Gpr183* on the pulmonary cDC2s in mice for the first time but also further quantified the role of *Gpr183* on the specific subset of cDC2s (CD301b⁺ cDC2s) which is informative for studying the role of GPR183 on human T-bet⁻ cDC2s.

4.3 Decrease in pulmonary cDC2 abundance is due to impaired proliferation and apoptosis

A balance of apoptosis and proliferation is critical for maintenance of cellular compartments. The reduction of pulmonary cDC2s in the absence of GPR183 suggests that GPR183 may regulate apoptosis or proliferation of cDC2s in the lung. We observed higher apoptosis and lower proliferation of cDC2s in the deficiency of GPR183. Impaired proliferation in the absence of GPR183 matches the data showing that *Gpr183*⁺ cDC2 shows higher proliferation profiles than their negative counterparts indicating that GPR183 is important for keeping cDC2 proliferation. These observations are contrary to previous publications showing that GPR183 neither regulates proliferation nor regulates apoptosis of splenic cDCs^[52]. One reason to explain this discrepancy could be that GPR183 has different roles on cDC2s within different tissues, as additional tissue specific factors act on either cDC2 or pre-cDC2, such as the previously published tissue specific signals lymphotoxin alpha 1 beta 2 (LT α 1 β 2) in the lymphoid organ or NOTCH2 in the intestine^[97, 98].

4.4 Decreased pulmonary cDC2s does not affect influx of pre-cDC2s in the lung

The development of cDCs follows a stepwise manner in the BM. Pre-cDCs from the BM seed in tissues and differentiate into cDCs within distinct microanatomical tissue niches. It was reported that GPR183 was not responsible for promoting the development of splenic cDC2s^[52, 57]. In line with this, although a specific decreased number of cDC2s was found in the lung of *Gpr183* deficient mice, the development of pre-cDCs, occurred in a normal manner in the BM, blood, and lung in the absence of *Gpr183*, which implied that the influx and the development of preDC in the lung was not affected by *Gpr183*. Accordingly, with the expression of *Gpr183* on early DC progenitors, we found normal frequencies of MDP and CDP in the BM of *Gpr183* deficient mice. Furthermore, cDC1s and cDC2s were generated normally from *Gpr183* deficient BM *in vitro*. Together, these evidence indicate that *Gpr183* does not seem to directly influence the development of cDCs *in vivo* and *in vitro*.

4.5 Decreased pulmonary cDC2s influence the migratory cDC2s in the draining LN

One of the functions of cDCs is migrating to LN and priming T cells via MHC2 antigen presentation^[99, 100]. *Gpr183*⁺ cDC2s showed a higher expression of MHC2 compared to *Gpr183*⁻ cDC2s, indicating that *Gpr183*⁺ cDC2s are potentially more potent in antigen presentation. Importantly, we found less migratory cDC2s in the lung draining-LN of *Gpr183* deficient mice, which is expected as an overall reduction of cDC2s in the lung was found in the *Gpr183* deficient mice. In the spleen, the reduction of cDC2s from *Gpr183* deficient mice contributes to a marked decrease in OTII T cell proliferation^[57]. In

addition, cDC1s were not able to compensate for a grossly smaller cDC2s subset in the spleen^[52]. This implies that the T cell priming function of the remaining migratory cDC2s might also be affected as the low number of migratory cDC2s could diminish the efficiency of antigen presentation and loading. Functional studies need to be performed to elucidate in detail.

4.6 Fibroblasts are the main producers of GPR183 ligand in the lung and GPR183 – 7 α ,25-OHC axis is important to keep cDC2s maintenance.

Determining the source of GPR183 ligands is critical to investigate which cell population interacts with pulmonary cDC2 and where the spatial niche exists in the lung. As a most potent GPR183 ligand, 7 α ,25-OHC is generated by sequential hydroxylation of cholesterol by CH25H and Cyp7b1. Previous research has shown that stromal cells and fibroblastic cells are the main producers of GPR183 ligands in the lymphoid tissue and intestine^[72, 101]. We found that PDGFR α ⁺Sca-1⁺ adventitial fibroblasts^[79] are the only stromal cells expressing both *Ch25h* and *Cyp7b1* in the lung, which are the two key enzymes generating GPR183 ligands. In mice unable to synthesize 7 α ,25-OHC (*Ch25h* and *Cyp7b1* deficiency)^[72, 102] has been suggested that the critical function of GPR183 ligands in splenic cDC2s is to mediate their maintenance and correct positioning^[52]. We found that *Ch25h* deficiency decreased pulmonary cDC2s and CD301b⁺ cDC2s, phenocopying *Gpr183* KO mice, which was expected as *Ch25h* is a key enzyme for producing GPR183 ligands. Interestingly, the defect of cDC2s in *Ch25h*^{-/-} mice was less severe than in *Gpr183*^{-/-} mice, most likely as a result of a compensatory mechanism driven by alternative GPR183 ligands such as 7 α ,27-OHC, which is produced

independently of CH25H^[71]. Altogether, we found that *Gpr183* and its ligands were required for the maintenance of pulmonary cDC2s and CD301b⁺ cDC2s. Although residual cDC2s were present in *Gpr183*^{-/-} and *Ch25h*^{-/-} mice, these cDC2s might be negative of GPR183.

4.7 Niche factor, TSLP produced by adventitial fibroblasts is critical to keep pulmonary cDC2s maintenance.

All the pulmonary mononuclear phagocytes, including cDC2s express *Gpr183*, and all of them are able to sense $7\alpha,25$ -OHC gradient generated by adventitial fibroblasts. But only cDC2s were affected by *Gpr183*, which indicate that besides *Gpr183*, there are probably other potential factors acting on cDC2s maintenance. For example, after migrating to fibroblasts, cDC2s might interact with fibroblasts and receive additional survival signals.

It was shown that GPR183 acts by promoting the differentiation or maintenance of cDC2s through its ability to regulate their localization in the spleen. GPR183⁺ cDC2s sense gradients of $7\alpha,25$ -OHC and migrate to the splenic marginal zone and bridging channels^[52] where B cells are enriched and able to produce lymphotoxin- $\alpha1\beta2$ ^[103], a membrane cytokine known to be required for the homeostasis of cDC2s^[97]. A similar model of regulation by GPR183 was proposed in the colon. Local generation of $7\alpha,25$ -OHC by fibroblastic stromal cells attracts GPR183-expressing group 3 innate lymphoid cells (ILC3s) to sites of cryptopatches formation. This process positions lymphotoxin- $\alpha1\beta2$ ⁺ ILC3s for crosstalk with lymphotoxin-bR⁺ stromal cells, which promotes the recruitment of GPR183-expressing B cells, to complete isolated lymphoid follicles (ILF) formation^[73]. If spatially restricted factors present in the lung are indeed required for the

maintenance of cDC2s, one possible source of these factors is fibroblasts, as they are producers of key enzymes in charge of synthesizing GPR183 ligands.

To find such a candidate factor in the pulmonary fibroblasts, we referred to public resources of RNAseq data from the mice lungs^[79, 91] and performed nichenet analysis which models intercellular communication by linking ligands to target receptor genes^[78]. We found that thymic stromal lymphopoietin (*Tslp*), expressed in fibroblasts, and cytokine receptor-like factor 2 (*Crlf2*), expressed by cDC2s, showed the highest interaction potential. TSLP is an IL-7-like cytokine produced by many cell types including epithelial cells, keratinocytes, and fibroblasts in the context of inflammation or infection^[104]. TSLP has been shown to stimulate DCs and further induce adaptive immune-mediated type 2 airway inflammation^[92, 93]. DC-specific ablation of *Tslpr* Mice showed selectively decreased numbers of CD301b⁺ cDC2s, indicating that TSLP-TSLPR is critical in regulating cDC2s. Rather than directly promoting the generation of cDC2s via yet-unknown signaling pathways, GPR183 may instead guide pulmonary cDC2s to the appropriate microanatomical niche where spatially restricted cues (TSLP) are ultimately responsible for driving differentiation or maintenance.

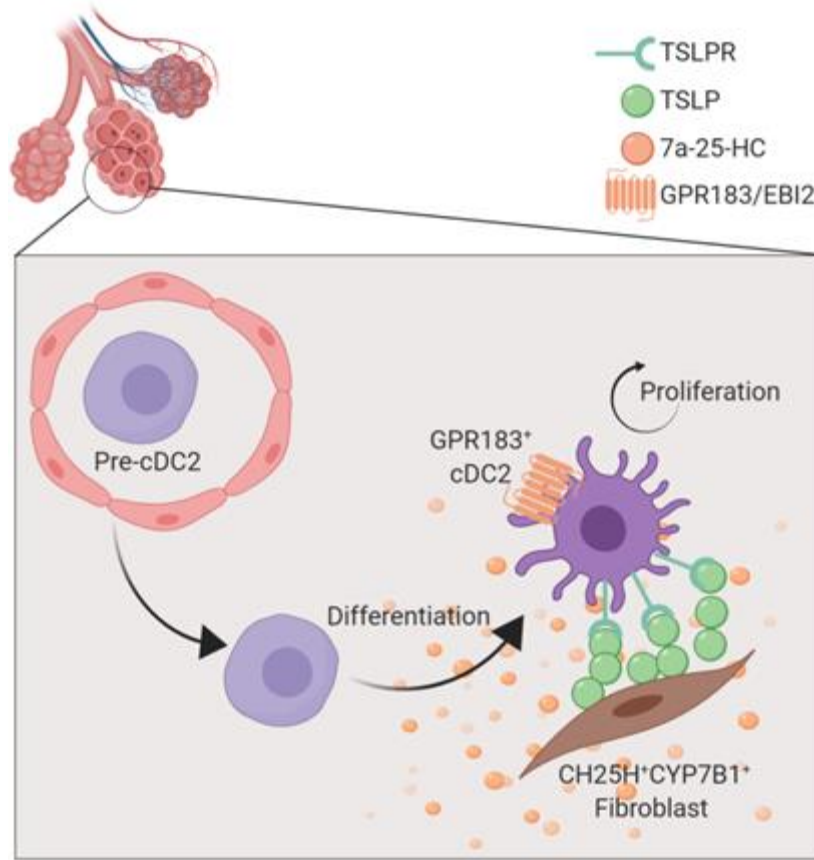


Figure 4-1. Model of cDC2 positioning and maintenance within the murine lung. Pre-cDC2s from bloodstream seed in the lung and differentiate into cDC2s with appropriate cytokines like FLT3L. GPR183⁺ cDC2s sense 7 α ,25-OHC generated by CH25H⁺CYP7B1⁺ fibroblasts and migrate to fibroblasts where they receive additional signals (TSLP produced by fibroblasts) that influence cDC2s maintenance (proliferation/apoptosis).

Based on the above evidence, we propose a model of GPR183-directed niche modulating cDC2s (**Fig. 4-1**). Pre-cDC2s arising from the BM, go into the bloodstream, and finally seed in the lung. pre-cDC2s differentiate into cDC2s via the action of cytokines like FLT3L. GPR183⁺ cDC2s sense 7 α ,25-OHC generated by CH25H⁺CYP7B1⁺ fibroblasts and migrate to fibroblasts where they have access to

TSLP. TSLP produced by fibroblasts stimulates cDC2s via TSLPR/CRLF2 (TSLPR) and keeps their maintenance.

Our study has extended the knowledge of the roles of GPR183 in the immune response. We have identified GPR183 as the chemotactic receptor responsible for the accumulation of cDC2s near the adventitial fibroblasts in the lung, and TSLP as a candidate niche factor required for the homeostasis of pulmonary cDC2s. This evidence may be valuable in designing DC-based vaccines and in evaluating the therapeutic benefits of oxysterols- GPR183. Our research has established broader functions of the GPR183- $7\alpha,25$ -OHC axis by linking GPR183-mediated cDC2s positioning to niche related maintenance of cDC2s during steady-state homeostasis. Future studies will need to define how infection or inflammation alters the tissue niches that support the maintenance of cDC2s and how cDC2s will be educated under altered tissue.

5 Acknowledgements

I enjoyed my PhD training and It was a great PhD journey! I am grateful for my supervisors, all the colleagues, friends, and family who gave me huge support physically and mentally in the past four years. Without any of you, I would not have reached there.

Prof. Andreas Schlitzer First of all, I would like to thank Andreas who recruited me from China. I will never forget how we met each other at the beginning. You are always supportive and encourage me greatly in this project. I am willing to try new experiments and learn new skills, and you always have new ideas which fit my curiosity. Thanks a lot for making my research stay in Japan and Spain possible where I gained various scientific view.

Besides scientific guiding, I got lots of care and privilege as a foreigner which made it easier for me to start at the beginning and adapt myself as fast as possible in Germany. I really appreciate all your kind, sweet, and thoughtful moments you have built in my memory.

Prof. Alexander Pfeifer and Prof. Christa E. Müller Without Prof. Pfeifer, I would not have been able to start this project. I really appreciate that you kindly donated different precious mice lines and suggestions are always good and helpful. It is an honor to have Prof. Müller as my second supervisor. With you supervision, our project will for sure go to a higher level.

GRK graduate school We got a lot of freedom to organize everything within all the members. Thanks to our coordinator **Elisabeth** for organizing everything perfectly. The scientific progress report twice per year prepared myself for any project presentation.

Combination of ways to train us as proper scientists was very helpful. I would definitely recommend it to my friends who intend to do a PhD in Germany.

Lab members I am very lucky to have such good colleagues to work with. You made my lab-life quite wonderful. Special thanks to **Mohamed** as we supported each other and help each other for many experiments, especially the experiments which were done during the weekend. Special thanks to **Jiangyan** as you are an amazing bioinformatics, takes care of RNAseq analyzing, and contributes a critical part for this project. Special thanks to **David** for sure as it was a huge help from you to do the correction for my thesis and you always encourage me a lot to go through this tough process.

Prof. Steven F. Ziegler I would like to express deepest appreciation to have collaboration with you. Thanks to Sabine for generating great and precious data which push my project even further.

Family and Friends I am happy to make new friends in Germany. Thanks a lot for your high tolerance as I am often late for parties or even not able to join the party. My parents who had no chance to fulfil their education as high as possible encouraged me and supported me to go for higher education in different cities in China, even abroad. I greatly appreciate all your support. I am sure you will never read my thesis because of the language barrier, but I am sure you are proud of me as your daughter is the only one who did a PhD in the whole family. Endless love from you always makes me feel safe. Last, but not the least, thanks to my husband Weicheng for taking care of me. Without you, I would not survive in Germany.

6 Reference

1. Forster, R., *et al.* CCR7 and its ligands: balancing immunity and tolerance. *Nat Rev Immunol*, 2008. **8**(5): 362-71.
2. Ohl, L., *et al.* CCR7 governs skin dendritic cell migration under inflammatory and steady-state conditions. *Immunity*, 2004. **21**(2): 279-88.
3. Banchereau, J.&Steinman, R. M. Dendritic cells and the control of immunity. *Nature*, 1998. **392**(6673): 245-52.
4. Steinman, R. M.&Cohn, Z. A. Identification of a novel cell type in peripheral lymphoid organs of mice. I. Morphology, quantitation, tissue distribution. *J Exp Med*, 1973. **137**(5): 1142-62.
5. Musumeci, A., *et al.* What Makes a pDC: Recent Advances in Understanding Plasmacytoid DC Development and Heterogeneity. *Front Immunol*, 2019. **10**: 1222.
6. Zhan, Y., *et al.* Plasmacytoid dendritic cells are short-lived: reappraising the influence of migration, genetic factors and activation on estimation of lifespan. *Sci Rep*, 2016. **6**: 25060.
7. Cisse, B., *et al.* Transcription factor E2-2 is an essential and specific regulator of plasmacytoid dendritic cell development. *Cell*, 2008. **135**(1): 37-48.
8. Grajkowska, L. T., *et al.* Isoform-Specific Expression and Feedback Regulation of E Protein TCF4 Control Dendritic Cell Lineage Specification. *Immunity*, 2017. **46**(1): 65-77.
9. Reizis, B. Plasmacytoid Dendritic Cells: Development, Regulation, and Function. *Immunity*, 2019. **50**(1): 37-50.

10. Guilliams, M., *et al.* Unsupervised High-Dimensional Analysis Aligns Dendritic Cells across Tissues and Species. *Immunity*, 2016. **45**(3): 669-684.
11. Satpathy, A. T., *et al.* Zbtb46 expression distinguishes classical dendritic cells and their committed progenitors from other immune lineages. *J Exp Med*, 2012. **209**(6): 1135-52.
12. Silva, R. G., *et al.* New silica gel-based monolithic column for nano-liquid chromatography, used in the HILIC mode. *J Chromatogr Sci*, 2012. **50**(8): 649-57.
13. Guilliams, M., *et al.* Dendritic cells, monocytes and macrophages: a unified nomenclature based on ontogeny. *Nat Rev Immunol*, 2014. **14**(8): 571-8.
14. Merad, M., *et al.* The dendritic cell lineage: ontogeny and function of dendritic cells and their subsets in the steady state and the inflamed setting. *Annu Rev Immunol*, 2013. **31**: 563-604.
15. Ginhoux, F., *et al.* The origin and development of nonlymphoid tissue CD103+ DCs. *J Exp Med*, 2009. **206**(13): 3115-30.
16. Taylor, P., *et al.* The BXH2 mutation in IRF8 differentially impairs dendritic cell subset development in the mouse. *Blood*, 2008. **111**(4): 1942-5.
17. Hildner, K., *et al.* Batf3 deficiency reveals a critical role for CD8alpha+ dendritic cells in cytotoxic T cell immunity. *Science*, 2008. **322**(5904): 1097-100.
18. Edelson, B. T., *et al.* Peripheral CD103+ dendritic cells form a unified subset developmentally related to CD8alpha+ conventional dendritic cells. *J Exp Med*, 2010. **207**(4): 823-36.

19. Hacker, C., *et al.* Transcriptional profiling identifies Id2 function in dendritic cell development. *Nat Immunol*, 2003. **4**(4): 380-6.
20. Sancho, D., *et al.* Identification of a dendritic cell receptor that couples sensing of necrosis to immunity. *Nature*, 2009. **458**(7240): 899-903.
21. Theisen, D. J., *et al.* WDFY4 is required for cross-presentation in response to viral and tumor antigens. *Science*, 2018. **362**(6415): 694-699.
22. Martinez-Lopez, M., *et al.* Batf3-dependent CD103+ dendritic cells are major producers of IL-12 that drive local Th1 immunity against *Leishmania major* infection in mice. *Eur J Immunol*, 2015. **45**(1): 119-29.
23. Desch, A. N., *et al.* CD103+ pulmonary dendritic cells preferentially acquire and present apoptotic cell-associated antigen. *J Exp Med*, 2011. **208**(9): 1789-97.
24. Dougherty, J. E. The role of hyperbaric oxygen therapy in crush injuries. *Crit Care Nurs Q*, 2013. **36**(3): 299-309.
25. Williams, J. W., *et al.* Transcription factor IRF4 drives dendritic cells to promote Th2 differentiation. *Nat Commun*, 2013. **4**: 2990.
26. Schlitzer, A., *et al.* IRF4 transcription factor-dependent CD11b+ dendritic cells in human and mouse control mucosal IL-17 cytokine responses. *Immunity*, 2013. **38**(5): 970-83.
27. Caton, M. L., *et al.* Notch-RBP-J signaling controls the homeostasis of CD8-dendritic cells in the spleen. *J Exp Med*, 2007. **204**(7): 1653-64.
28. Lewis, K. L., *et al.* Notch2 receptor signaling controls functional differentiation of dendritic cells in the spleen and intestine. *Immunity*, 2011. **35**(5): 780-91.

29. Tussiwand, R., *et al.* Klf4 expression in conventional dendritic cells is required for T helper 2 cell responses. *Immunity*, 2015. **42**(5): 916-28.
30. Gao, Y., *et al.* Control of T helper 2 responses by transcription factor IRF4-dependent dendritic cells. *Immunity*, 2013. **39**(4): 722-32.
31. Woolf, D. K., *et al.* Fractionated stereotactic radiotherapy for acoustic neuromas: long-term outcomes. *Clin Oncol (R Coll Radiol)*, 2013. **25**(12): 734-8.
32. Briseno, C. G., *et al.* Notch2-dependent DC2s mediate splenic germinal center responses. *Proc Natl Acad Sci U S A*, 2018. **115**(42): 10726-10731.
33. Brown, C. C., *et al.* Transcriptional Basis of Mouse and Human Dendritic Cell Heterogeneity. *Cell*, 2019. **179**(4): 846-863 e24.
34. Kumamoto, Y., *et al.* CD301b(+) dermal dendritic cells drive T helper 2 cell-mediated immunity. *Immunity*, 2013. **39**(4): 733-43.
35. Kumamoto, Y., *et al.* CD301b(+) dendritic cells suppress T follicular helper cells and antibody responses to protein antigens. *Elife*, 2016. **5**.
36. Bosteels, C., *et al.* Inflammatory Type 2 cDCs Acquire Features of cDC1s and Macrophages to Orchestrate Immunity to Respiratory Virus Infection. *Immunity*, 2020. **52**(6): 1039-1056 e9.
37. Liu, K.&Nussenzweig, M. C. Origin and development of dendritic cells. *Immunol Rev*, 2010. **234**(1): 45-54.
38. Sichen, D., *et al.* IRF8 Transcription Factor Controls Survival and Function of Terminally Differentiated Conventional and Plasmacytoid Dendritic Cells, Respectively. *Immunity*, 2016. **45**(3): 626-640.

39. Onai, N., *et al.* Identification of clonogenic common Flt3+M-CSFR+ plasmacytoid and conventional dendritic cell progenitors in mouse bone marrow. *Nat Immunol*, 2007. **8**(11): 1207-16.
40. Naik, S. H., *et al.* Development of plasmacytoid and conventional dendritic cell subtypes from single precursor cells derived in vitro and in vivo. *Nat Immunol*, 2007. **8**(11): 1217-26.
41. Miller, J. C., *et al.* Deciphering the transcriptional network of the dendritic cell lineage. *Nat Immunol*, 2012. **13**(9): 888-99.
42. Schlitzer, A., *et al.* Identification of cDC1- and cDC2-committed DC progenitors reveals early lineage priming at the common DC progenitor stage in the bone marrow. *Nat Immunol*, 2015. **16**(7): 718-28.
43. Grajales-Reyes, G. E., *et al.* Batf3 maintains autoactivation of Irf8 for commitment of a CD8alpha(+) conventional DC clonogenic progenitor. *Nat Immunol*, 2015. **16**(7): 708-17.
44. Persson, E. K., *et al.* IRF4 transcription-factor-dependent CD103(+)CD11b(+) dendritic cells drive mucosal T helper 17 cell differentiation. *Immunity*, 2013. **38**(5): 958-69.
45. Waskow, C., *et al.* The receptor tyrosine kinase Flt3 is required for dendritic cell development in peripheral lymphoid tissues. *Nat Immunol*, 2008. **9**(6): 676-83.
46. McKenna, H. J., *et al.* Mice lacking flt3 ligand have deficient hematopoiesis affecting hematopoietic progenitor cells, dendritic cells, and natural killer cells. *Blood*, 2000. **95**(11): 3489-97.

47. Sichien, D., *et al.* Development of conventional dendritic cells: from common bone marrow progenitors to multiple subsets in peripheral tissues. *Mucosal Immunol*, 2017. **10**(4): 831-844.
48. Poltorak, M. P.&Schraml, B. U. Fate mapping of dendritic cells. *Front Immunol*, 2015. **6**: 199.
49. Murphy, T. L., *et al.* Transcriptional Control of Dendritic Cell Development. *Annu Rev Immunol*, 2016. **34**: 93-119.
50. Allard, B., *et al.* Alveolar Macrophages in the Resolution of Inflammation, Tissue Repair, and Tolerance to Infection. *Front Immunol*, 2018. **9**: 1777.
51. Lyons-Cohen, M. R., *et al.* Precision-cut Mouse Lung Slices to Visualize Live Pulmonary Dendritic Cells. *J Vis Exp*, 2017(122).
52. Gatto, D., *et al.* The chemotactic receptor EBI2 regulates the homeostasis, localization and immunological function of splenic dendritic cells. *Nat Immunol*, 2013. **14**(5): 446-53.
53. Rosenkilde, M. M., *et al.* Molecular pharmacological phenotyping of EBI2. An orphan seven-transmembrane receptor with constitutive activity. *J Biol Chem*, 2006. **281**(19): 13199-208.
54. Stepien, T., *et al.* Morphological and quantitative analysis of cerebellar cortical cells in Alzheimer's disease. *Folia Neuropathol*, 2012. **50**(3): 250-60.
55. GeurtsvanKessel, C. H.&Lambrecht, B. N. Division of labor between dendritic cell subsets of the lung. *Mucosal Immunol*, 2008. **1**(6): 442-50.
56. Wyss, A., *et al.* The EBI2-oxysterol axis promotes the development of intestinal lymphoid structures and colitis. *Mucosal Immunol*, 2019. **12**(3): 733-745.

57. Yi, T.&Cyster, J. G. EB12-mediated bridging channel positioning supports splenic dendritic cell homeostasis and particulate antigen capture. *Elife*, 2013. **2**: e00757.
58. Hannedouche, S., *et al.* Oxysterols direct immune cell migration via EB12. *Nature*, 2011. **475**(7357): 524-7.
59. Liu, C., *et al.* Oxysterols direct B-cell migration through EB12. *Nature*, 2011. **475**(7357): 519-23.
60. Benned-Jensen, T., *et al.* Ligand modulation of the Epstein-Barr virus-induced seven-transmembrane receptor EB12: identification of a potent and efficacious inverse agonist. *J Biol Chem*, 2011. **286**(33): 29292-302.
61. Luttrell, L. M.&Gesty-Palmer, D. Beyond desensitization: physiological relevance of arrestin-dependent signaling. *Pharmacol Rev*, 2010. **62**(2): 305-30.
62. Gessier, F., *et al.* Identification and characterization of small molecule modulators of the Epstein-Barr virus-induced gene 2 (EB12) receptor. *J Med Chem*, 2014. **57**(8): 3358-68.
63. Benned-Jensen, T., *et al.* Small molecule antagonism of oxysterol-induced Epstein-Barr virus induced gene 2 (EB12) activation. *FEBS Open Bio*, 2013. **3**: 156-60.
64. Rutkowska, A., *et al.* The Role of the Oxysterol/EB12 Pathway in the Immune and Central Nervous Systems. *Curr Drug Targets*, 2016. **17**(16): 1851-1860.
65. Gatto, D., *et al.* Guidance of B cells by the orphan G protein-coupled receptor EB12 shapes humoral immune responses. *Immunity*, 2009. **31**(2): 259-69.

66. Pereira, J. P., *et al.* EBI2 mediates B cell segregation between the outer and centre follicle. *Nature*, 2009. **460**(7259): 1122-6.
67. Wanke, F., *et al.* EBI2 Is Highly Expressed in Multiple Sclerosis Lesions and Promotes Early CNS Migration of Encephalitogenic CD4 T Cells. *Cell Rep*, 2017. **18**(5): 1270-1284.
68. Rutkowska, A., *et al.* EBI2 regulates pro-inflammatory signalling and cytokine release in astrocytes. *Neuropharmacology*, 2018. **133**: 121-128.
69. Shen, Z. J., *et al.* Epstein-Barr Virus-induced Gene 2 Mediates Allergen-induced Leukocyte Migration into Airways. *Am J Respir Crit Care Med*, 2017. **195**(12): 1576-1585.
70. Li, J., *et al.* EBI2 augments Tfh cell fate by promoting interaction with IL-2- quenching dendritic cells. *Nature*, 2016. **533**(7601): 110-4.
71. Lu, E., *et al.* Distinct oxysterol requirements for positioning naive and activated dendritic cells in the spleen. *Sci Immunol*, 2017. **2**(10).
72. Yi, T., *et al.* Oxysterol gradient generation by lymphoid stromal cells guides activated B cell movement during humoral responses. *Immunity*, 2012. **37**(3): 535-48.
73. Emgard, J., *et al.* Oxysterol Sensing through the Receptor GPR183 Promotes the Lymphoid-Tissue-Inducing Function of Innate Lymphoid Cells and Colonic Inflammation. *Immunity*, 2018. **48**(1): 120-132 e8.
74. Baptista, A. P., *et al.* The Chemoattractant Receptor Ebi2 Drives Intranodal Naive CD4(+) T Cell Peripheralization to Promote Effective Adaptive Immunity. *Immunity*, 2019. **50**(5): 1188-1201 e6.

75. Suan, D., *et al.* T follicular helper cells have distinct modes of migration and molecular signatures in naive and memory immune responses. *Immunity*, 2015. **42**(4): 704-18.
76. Kelly, L. M., *et al.* EB12 guides serial movements of activated B cells and ligand activity is detectable in lymphoid and nonlymphoid tissues. *J Immunol*, 2011. **187**(6): 3026-32.
77. Tang, J., *et al.* Downregulation of GPR183 on infection restricts the early infection and intracellular replication of mycobacterium tuberculosis in macrophage. *Microb Pathog*, 2020. **145**: 104234.
78. Browaeys, R., *et al.* NicheNet: modeling intercellular communication by linking ligands to target genes. *Nat Methods*, 2020. **17**(2): 159-162.
79. Tsukui, T., *et al.* Collagen-producing lung cell atlas identifies multiple subsets with distinct localization and relevance to fibrosis. *Nat Commun*, 2020. **11**(1): 1920.
80. Scott, C. L., *et al.* CCR2(+)/CD103(-) intestinal dendritic cells develop from DC-committed precursors and induce interleukin-17 production by T cells. *Mucosal Immunol*, 2015. **8**(2): 327-39.
81. Liu, Z., *et al.* Fate Mapping via Ms4a3-Expression History Traces Monocyte-Derived Cells. *Cell*, 2019. **178**(6): 1509-1525 e19.
82. Becht, E., *et al.* Dimensionality reduction for visualizing single-cell data using UMAP. *Nat Biotechnol*, 2018.

83. Hirao, M., *et al.* CC chemokine receptor-7 on dendritic cells is induced after interaction with apoptotic tumor cells: critical role in migration from the tumor site to draining lymph nodes. *Cancer Res*, 2000. **60**(8): 2209-17.
84. Cavanagh, L. L., *et al.* Proliferation in monocyte-derived dendritic cell cultures is caused by progenitor cells capable of myeloid differentiation. *Blood*, 1998. **92**(5): 1598-607.
85. Segura, E., *et al.* Characterization of resident and migratory dendritic cells in human lymph nodes. *J Exp Med*, 2012. **209**(4): 653-60.
86. Melillo, J. A., *et al.* Dendritic cell (DC)-specific targeting reveals Stat3 as a negative regulator of DC function. *J Immunol*, 2010. **184**(5): 2638-45.
87. Park, S. J., *et al.* IL-6 regulates in vivo dendritic cell differentiation through STAT3 activation. *J Immunol*, 2004. **173**(6): 3844-54.
88. Bell, B. D., *et al.* The transcription factor STAT5 is critical in dendritic cells for the development of TH2 but not TH1 responses. *Nat Immunol*, 2013. **14**(4): 364-71.
89. Eddy, W. E., *et al.* Stat5 Is Required for CD103(+) Dendritic Cell and Alveolar Macrophage Development and Protection from Lung Injury. *J Immunol*, 2017. **198**(12): 4813-4822.
90. Zhou, B., *et al.* The angiocrine Rspodin3 instructs interstitial macrophage transition via metabolic-epigenetic reprogramming and resolves inflammatory injury. *Nat Immunol*, 2020. **21**(11): 1430-1443.
91. Raredon, M. S. B., *et al.* Single-cell connectomic analysis of adult mammalian lungs. *Sci Adv*, 2019. **5**(12): eaaw3851.

92. Ito, T., *et al.* TSLP-activated dendritic cells induce an inflammatory T helper type 2 cell response through OX40 ligand. *J Exp Med*, 2005. **202**(9): 1213-23.
93. Kabata, H., *et al.* Targeted deletion of the TSLP receptor reveals cellular mechanisms that promote type 2 airway inflammation. *Mucosal Immunol*, 2020. **13**(4): 626-636.
94. Belz, G. T.&Nutt, S. L. Transcriptional programming of the dendritic cell network. *Nat Rev Immunol*, 2012. **12**(2): 101-13.
95. Kim, H. P., *et al.* Transcriptional and epigenetic networks in the development and maturation of dendritic cells. *Epigenomics*, 2013. **5**(2): 195-204.
96. Black, M. M. Prurigo of pregnancy, papular dermatitis of pregnancy, and pruritic folliculitis of pregnancy. *Semin Dermatol*, 1989. **8**(1): 23-5.
97. Kabashima, K., *et al.* Intrinsic lymphotoxin-beta receptor requirement for homeostasis of lymphoid tissue dendritic cells. *Immunity*, 2005. **22**(4): 439-50.
98. Satpathy, A. T., *et al.* Notch2-dependent classical dendritic cells orchestrate intestinal immunity to attaching-and-effacing bacterial pathogens. *Nat Immunol*, 2013. **14**(9): 937-48.
99. Turley, S. J., *et al.* Transport of peptide-MHC class II complexes in developing dendritic cells. *Science*, 2000. **288**(5465): 522-7.
100. Boes, M., *et al.* T-cell engagement of dendritic cells rapidly rearranges MHC class II transport. *Nature*, 2002. **418**(6901): 983-8.
101. Chu, C., *et al.* Anti-microbial Functions of Group 3 Innate Lymphoid Cells in Gut-Associated Lymphoid Tissues Are Regulated by G-Protein-Coupled Receptor 183. *Cell Rep*, 2018. **23**(13): 3750-3758.

102. Russell, D. W. The enzymes, regulation, and genetics of bile acid synthesis. *Annu Rev Biochem*, 2003. **72**: 137-74.
103. Ansel, K. M., *et al.* A chemokine-driven positive feedback loop organizes lymphoid follicles. *Nature*, 2000. **406**(6793): 309-14.
104. Ziegler, S. F., *et al.* The biology of thymic stromal lymphopoietin (TSLP). *Adv Pharmacol*, 2013. **66**: 129-55.

Summary

We found that the absence of GPR183 resulted in a specific decrease of the resident pulmonary cDC2 population due to impaired *in situ* proliferation and increased apoptosis. In contrast, development of DC was not affected by GPR183 ablation. Furthermore, analysis of the CH25H deficient mice revealed that CH25H dependent production of 7 α ,25-OHC is crucial for pulmonary cDC2 homeostasis. Adventitial fibroblasts are the major producer of 7 α ,25-OHC in the lung. Therefore we assessed the subtissular location of pulmonary cDC2 in the lung. This analysis revealed that cDC2 closely associate, in a GPR183 dependent manner, with adventitial fibroblasts. Next using single-cell transcriptomic data and cellular interaction modeling, we identified the TSLP – TSLPR axis as a possible candidate promoting cDC2 survival in a GPR183 dependent manner. Accordingly, DC-specific TSLPR KO mice had decreased pulmonary cDC2s numbers.

Collectively these findings demonstrate that GPR183 plays an intrinsic role in cDC2 maintenance and reveals GPR183 as a crucial regulator of peripheral organ resident DC homeostasis and subtissular location. What is more, GPR183 – 7 α ,25-OHC acts as a guiding axis for pulmonary cDC2 localizing in their supporting subtissular niche where cDC2 has an access to pro-survival factors such as TSLP instructed by fibroblast.

PUBLICATIONS

1. Weier A, Homrich M, Ebbinghaus S,... **Zhang L**, *et al.* Amplified centrosomes enhance migration and immune cell effector functions of mature dendritic cells. *Nature*. 2021. (preprint)
2. Xu H, Cai L, Li Z, **Zhang L**, *et al.* Dual effect of IL-7/IL-7R signalling on the osteoimmunological system: a potential therapeutic target for rheumatoid arthritis. *Immunology*. 2021.
3. Xu H, Cai L, **Zhang L**, *et al.* Paeoniflorin ameliorates collagen-induced arthritis via suppressing nuclear factor- κ B signalling pathway in osteoclast differentiation. *Immunology*. Feb, 2018.
4. Zhang H, Qi Y, Yuan Y,... **Zhang L**, *et al.* Paeoniflorin ameliorates experimental autoimmune encephalomyelitis via inhibition of dendritic cell function and Th17 cell differentiation. *Sci Rep*. Feb, 2017.
5. Cai L, Xu H, Zhang H, **Zhang L**, *et al.* Blockade of IL-7R α alleviates collagen-induced arthritis via inhibiting Th1 cell differentiation and CD4⁺ T cell migration. *Mol Immunol*. Nov, 2016.

CONFERENCES

02.04-02.03.2021	(Talk) Meeting of the AK Dendritic Cells
11.09-11.10.2020	(Talk) ImmunoSensation Cluster Science Days
10.19-10.23.2019	(Talk) 17th Congress of the International Union of Immunological Societies
09.12-09.14.2019	(Poster) 33rd Conference of the European Macrophage and Dendritic cell Society
09.10 -09.14.2018	(talk) ImmunoSensation summer school
04.08-04.12.2018	(Poster) Keystone symposia on molecular and cellular biology, myeloid cells